9-18-2006

Maximum Likelihood Estimation of Compound-Gaussian Clutter and Target Parameters

Jian Wang
The University of Illinois at Chicago

Aleksandar Dogandžić
Iowa State University, ald@iastate.edu

Arye Nehorai
The University of Illinois at Chicago

Maximum Likelihood Estimation of Compound-Gaussian Clutter and Target Parameters

Jian Wang [†] Aleksandar Dogandžić [‡] and Arye Nehorai [†]

[†] ECE Department, University of Illinois at Chicago, 851 S. Morgan St., Chicago, IL 60607

[‡] ECpE Department, Iowa State University, 3119 Coover Hall, Ames, IA 50011

Email: {jwang,nehorai}@ece.uic.edu ald@iastate.edu

Abstract

Compound-Gaussian models are used in radar signal processing to describe heavy-tailed clutter distributions. The important problems in compound-Gaussian clutter modeling are choosing the texture distribution, and estimating its parameters. Many texture distributions have been studied, and their parameters are typically estimated using statistically suboptimal approaches. We develop maximum likelihood (ML) methods for jointly estimating the target and clutter parameters in compound-Gaussian clutter using radar array measurements. In particular, we estimate (i) the complex target amplitudes, (ii) a spatial and temporal covariance matrix of the speckle component, and (iii) texture distribution parameters. Parameter-expanded expectation-maximization (PX-EM) algorithms are developed to compute the ML estimates of the unknown parameters. We also derived the Cramér-Rao bounds (CRBs) and related bounds for these parameters. We first derive general CRB expressions under an arbitrary texture model then simplify them for specific texture distributions. We consider the widely used gamma texture model, and propose an inverse-gamma texture model, leading to a complex multivariate t clutter distribution and closed-form expressions of the CRB. We study the performance of the proposed methods via numerical simulations.

Index Terms

Compound-Gaussian model, estimation, Cramér-Rao bound, parameter-expanded expectation-maximization (PX-EM).

The work of J. Wang and A. Nehorai was supported by the Air Force Office of Scientific Research Grant F49620-02-1-0339 and DARPA/AFOSR Grant FA9550-04-1-0187.

I. INTRODUCTION

When a radar system illuminates a large area of the sea, the probability density function (pdf) of the amplitude of the returned signal is well approximated by the Rayleigh distribution [1], i.e., the echo can be modeled as a complex-Gaussian process. That distribution is a good approximation. This can be proved theoretically by the central limit theorem, since the returned signal can be viewed as the sum of the reflection from a large number of randomly-phased independent scatterers. However, in high-resolution and low-grazing-angle radar, the real clutter data show significant deviations from the complex Gaussian model, see [2], because only a small sea surface area is illuminated by the narrow radar beam. The behavior of the small patch is non-stationary [1] and the number of scatterers is random, see [3]. Due to the different waveform characteristics and generation mechanism, the sea surface wave, i.e., the roughness of the sea surface, is often modeled in two scales [4], [5]. To take into account different scales of roughness, a two-scale sea surface scattering model was developed, see [6], [7], [8]. In this two-scale model — a *compound-Gaussian* model — the fast-changing component, which accounts for local scattering, is referred to as *speckle* $\boldsymbol{\chi}(t)$. It is assumed to be a stationary complex Gaussian process with zero mean. The slow-changing component, *texture* $u(t)$ is used to describe the variation of the local power due to the tilting of the illuminated area, and it is modeled as a nonnegative real random process. The complex clutter can be written as the product of these two components

$$\boldsymbol{e}(t) = \sqrt{u(t)}\boldsymbol{\chi}(t) \tag{1}$$

The compound-Gaussian model is a model widely used to characterize the heavy-tailed clutter distributions in radar, especially sea clutter, see [2], [6], [9], and Section II. It belongs to the class of the spherically invariant random process (SIRP), see [10], [17]. Note that the compound-Gaussian distribution is also often used to model speech waveforms and various radio propagation channel disturbance, see [10] and the references therein.

Modeling of clutter using a compound-Gaussian distribution involves these important aspects: choosing the texture distribution, estimating its parameters, and evaluating the efficiency of the estimations. Many texture distributions have been studied, but their parameters were typically estimated using the method of moments, which is statistically suboptimal, see [2]. We present our measurement model in Section II. In Section III, we develop the parameter-expanded expectation-maximization (PX-EM) algorithms to estimate the target and clutter parameters. We compute the CRBs for the general compound-Gaussian model and simplify them for two texture distributions in Section IV. In Section V, we verify our results through Monte-Carlo numerical simulations.

II. MODELS

We extend the radar array measurement model in [11] to account for compound-Gaussian clutter. Assume that an n-element radar array receives P pulse returns, where each pulse provides N samples. We collect the spatio-temporal data from the tth range gate into a vector $\boldsymbol{y}(t)$ of size $m = nP$ and model $\boldsymbol{y}(t)$ as (see [11] and [12]) [1]

$$\boldsymbol{y}(t) = AX\boldsymbol{\phi}(t) + \boldsymbol{e}(t), \quad t = 1, \ldots, N, \tag{2}$$

where A is an $m \times r$ spatio-temporal steering matrix of the targets, $\Phi = [\boldsymbol{\phi}(1), \boldsymbol{\phi}(2), \ldots, \boldsymbol{\phi}(N)]$ is the temporal response matrix, X is an $r \times d$ matrix of unknown complex amplitudes of the targets. Here r is the number of possible directions that the reflection signals will come from, and d is the number of range gate that covers the target.[2] The additive noise vectors $\boldsymbol{e}(t), t = 1, 2, \ldots, N$ are independent, identically distributed (i.i.d.) and come from a compound-Gaussian probability distribution, see e.g. [3], [10] and [14]–[17].

We now represent the above measurement scenario using the following hierarchical model: $\boldsymbol{y}(t)$ are conditionally independent random vectors with probability density functions (pdfs):

$$p_{\boldsymbol{y}|u}(\boldsymbol{y}(t) \,|\, u(t); X, \Sigma) = \exp\left\{-[\boldsymbol{y}(t) - AX\boldsymbol{\phi}(t)]^H \cdot [u(t)\Sigma]^{-1} \cdot [\boldsymbol{y}(t) - AX\boldsymbol{\phi}(t)]\right\} \Big/ |\pi u(t)\Sigma|, \tag{3}$$

where the superscript "^{H}" denotes the Hermitian (conjugate) transpose, Σ is the (unknown) covariance matrix of the speckle component, and $u(t)$, $t = 1, 2, \ldots, N$ are the unobserved texture components (powers). We assume the texture to be fully correlated during the coherent processing interval (CPI) [18]. This assumption is reasonable since the radar processing time is not too long. We consider the following texture distributions:

- **gamma:** $u(t)$ follow a gamma distribution [2], [3], [14]
- **inverse gamma:** $1/u(t)$ follow a gamma distribution [19], [20], [21]

III. MAXIMUM LIKELIHOOD ESTIMATION

We develop the ML estimates of the complex amplitude matrix X, speckle covariance matrix Σ, and texture distribution parameter ν from the measurements $\boldsymbol{y} = [\boldsymbol{y}(1)^T, \boldsymbol{y}(2)^T, \ldots, \boldsymbol{y}(N)^T]^T$, see [22]. In the following, we present the PX-EM algorithms for ML estimation of these parameters under the above three texture models. The PX-EM algorithms share the same monotonic convergence properties as the "classical" expectation-maximization (EM) algorithms, see [23, Theorem 1]. They outperform the EM algorithms in the global rate of convergence, see [23, Theorem 2]. In our problem,

[1] A special case of the model (2) for rank-one targets (i.e., scalar X) in compound-Gaussian clutter was considered in [15].

[2] In high resolution radar, target can usually distribute in more than one range gates, see [13] and reference therein.

the computations are confined to the PX-E step of the PX-EM algorithm. The PX-M step follows as a straightforward consequence of the PX-E step.

A. PX-EM Algorithm for Gamma Texture

We model the texture components $u(t)$, $t = 1, 2, \ldots, N$ as gamma random variables with unit mean (as e.g. in [3]) and unknown shape parameter $\nu > 0$, i.e.,

$$p_u(u(t);\nu) = \frac{1}{\Gamma(\nu)} \cdot \nu^{\nu} u(t)^{\nu-1} \exp\big[-\nu u(t)\big]; \tag{4}$$

hence, the unknown parameters are $\boldsymbol{\theta} = \{X, \Sigma, \nu\}$. (The shape parameter ν is also known as the Nakagami-m parameter in the communications literature, see e.g. [24, Ch. 2.2.1.4].) This choice of texture distribution leads to the well-known K clutter model, see [2] and [3] and references therein.

The method for deriving EM- algorithm from complete-data sufficient statistics for a similar GMANOVA model is presented in [12]. Since EM algorithms often converge slowly in some situations, we propose a PX-EM algorithm. Because of the introduction of new parameter, PX-EM algorithm can capture extra information from the complete data in the PX-E step. Also because its M step performs a more efficient analysis by fitting the expanded model, PX-EM has a rate of convergence at least as fast as the parent EM [23].

The proposed PX-EM algorithm estimates $\boldsymbol{\theta}$ by treating $u(t)$, $t = 1, 2, \ldots, N$ as the unobserved data. First we add an auxiliary parameter μ_u (the mean of $u(t)$) to the set of parameters $\boldsymbol{\theta}$. Note that $\mu_u = 1$ in the original model. Hence the augmented parameter set is $\boldsymbol{\theta}_{\mathrm{a}} = \{X, \Sigma_{\mathrm{a}}, \nu, \mu_u\}$, where Σ_{a} and Σ are related as follows: $\Sigma = \mu_u \cdot \Sigma_{\mathrm{a}}$. Note that μ_u and Σ_{a} are not unique whereas their product Σ is. Under this expanded model, the pdf of $u(t)$ is (for $u(t) \geq 0$)

$$p_u(u(t);\nu,\mu_u) = \frac{1}{\Gamma(\nu)} \Big(\frac{\nu}{\mu_u}\Big)^{\nu} u(t)^{\nu-1} \exp\big[-\nu u(t)/\mu_u\big] \tag{5}$$

where $\Gamma(\cdot)$ denotes the gamma function. The conditional pdfs of $\boldsymbol{y}(t)$ are unchanged, see (3). The underlying statistical principle of PX-EM is to perform a "covariance adjustment" to correct the M step. In this problem, we adjust the covariance matrix Σ to a product of μ_u and Σ_{a}. More specifically, we use a expanded complete-data model that has a larger set of identifiable parameters, but leads to the original observed-data model with the original parameters identified from the expanded parameters via a many-to-one mapping [23].

We present the details of the derivation of the PX-EM algorithm in Appendix A. To summarize it, in the PX-E step, we calculate the conditional expectations of the complete-data sufficient statistics assuming all unknown parameters $\boldsymbol{\theta}_{\mathrm{a}}$ are known from the complete data log-likelihood. In the PX-M step, we estimate the unknown parameters from these expectations. The derivation of these estimates

from the sufficient statistics are explained in [12] in details. The PX-EM algorithm for the above expanded model consists of iterating between the following PX-E and PX-M steps:

PX-E Step: Compute the conditional expectations of the natural sufficient statistics

$$T_1(\boldsymbol{y};\boldsymbol{\theta}_{\rm a}^{(i)}) \;=\; \frac{1}{N}\cdot\sum_{t=1}^{N}\boldsymbol{y}(t)\boldsymbol{\phi}(t)^H\cdot \mathrm{E}_{\,u|y}[\,u(t)^{-1}\mid \boldsymbol{y}(t);\boldsymbol{\theta}_{\rm a}^{(i)}], \tag{6a}$$

$$T_2(\boldsymbol{y};\boldsymbol{\theta}_{\rm a}^{(i)}) \;=\; \frac{1}{N}\cdot\sum_{t=1}^{N}\boldsymbol{y}(t)\boldsymbol{y}(t)^H\cdot \mathrm{E}_{\,u|y}[\,u(t)^{-1}\mid \boldsymbol{y}(t);\boldsymbol{\theta}_{\rm a}^{(i)}], \tag{6b}$$

$$T_3(\boldsymbol{y};\boldsymbol{\theta}_{\rm a}^{(i)}) \;=\; \frac{1}{N}\cdot\sum_{t=1}^{N}\boldsymbol{\phi}(t)\boldsymbol{\phi}(t)^H\cdot \mathrm{E}_{\,u|y}[\,u(t)^{-1}\mid \boldsymbol{y}(t);\boldsymbol{\theta}_{\rm a}^{(i)}], \tag{6c}$$

$$t_4(\boldsymbol{y};\boldsymbol{\theta}_{\rm a}^{(i)}) \;=\; \frac{1}{N}\cdot\sum_{t=1}^{N}\mathrm{E}_{\,u|y}[\ln u(t)\mid \boldsymbol{y}(t);\boldsymbol{\theta}_{\rm a}^{(i)}], \tag{6d}$$

$$t_5(\boldsymbol{y};\boldsymbol{\theta}_{\rm a}^{(i)}) \;=\; \frac{1}{N}\cdot\sum_{t=1}^{N}\mathrm{E}_{\,u|y}[\,u(t)\mid \boldsymbol{y}(t);\boldsymbol{\theta}_{\rm a}^{(i)}], \tag{6e}$$

where $\boldsymbol{\theta}_{\rm a}^{(i)}=\{X^{(i)},\,\Sigma_{\rm a}^{(i)},\,\nu^{(i)},\,\mu_u^{(i)}\}$ is the estimate of $\boldsymbol{\theta}_{\rm a}$ in the ith iteration and (6a)–(6e) are computed using (8) (below) with $g(u(t))=u(t)^{-1},\ln u(t)$, and $u(t)$.

PX-M Step: Compute

$$X^{(i+1)} \;=\; [A^H(S^{(i)})^{-1}A]^{-1}A^H(S^{(i)})^{-1}\cdot T_1(\boldsymbol{y},\boldsymbol{\theta}_{\rm a}^{(i)})\,T_3(\boldsymbol{y},\boldsymbol{\theta}_{\rm a}^{(i)})^{-1}, \tag{7a}$$

$$\begin{aligned}\Sigma_{\rm a}^{(i+1)} \;&=\; S^{(i)}+[I_m-Q^{(i)}(S^{(i)})^{-1}]\,T_1(\boldsymbol{y},\boldsymbol{\theta}_{\rm a}^{(i)})\\ &\quad\cdot T_3(\boldsymbol{y};\boldsymbol{\theta}_{\rm a}^{(i)})^{-1}T_1(\boldsymbol{y},\boldsymbol{\theta}_{\rm a}^{(i)})^H\,[I_m-Q^{(i)}(S^{(i)})^{-1}]^H,\end{aligned} \tag{7b}$$

$$\mu_u^{(i+1)} \;=\; t_5(\boldsymbol{y},\boldsymbol{\theta}^{(i)}), \tag{7c}$$

$$\Sigma^{(i+1)} \;=\; \mu_u^{(i+1)}\cdot\Sigma_{\rm a}^{(i+1)}, \tag{7d}$$

where

$$S^{(i)} \;=\; T_2(\boldsymbol{y},\boldsymbol{\theta}_{\rm a}^{(i)})-T_1(\boldsymbol{y},\boldsymbol{\theta}_{\rm a}^{(i)})\cdot T_3(\boldsymbol{y};\boldsymbol{\theta}_{\rm a}^{(i)})^{-1}\cdot T_1(\boldsymbol{y},\boldsymbol{\theta}_{\rm a}^{(i)})^H, \tag{7e}$$

$$Q^{(i)} \;=\; A\,[A^H(S^{(i)})^{-1}A]^{-1}A^H, \tag{7f}$$

and find $\nu^{(i+1)}$ that maximizes

$$\nu^{(i+1)} \;=\; \arg\max_{\nu}\Big\{-\ln\Gamma(\nu)+\nu\ln\nu-\nu\ln[t_5(\boldsymbol{y},\boldsymbol{\theta}^{(i)})]+\nu t_4(\boldsymbol{y},\boldsymbol{\theta}^{(i)})-\nu\Big\}.$$

The above iteration is performed until $X^{(i)}$, $\Sigma^{(i)}$, and $\nu^{(i)}$ converge. The computation of $\nu^{(i+1)}$ requires maximizing (7c), which is accomplished using the Newton-Raphson method (embedded within the "outer" EM iteration, similar to [26]). The conditional-expectation expression (8) is obtained by using the Bayes rule, equations (3) and (4), and change-of-variable transformation $x=\nu u/\mu$.

$$\mathrm{E}_{\,u|\boldsymbol{y}}[g(u(t))\mid \boldsymbol{y}(t);\boldsymbol{\theta}_{\rm a}] = \frac{\int_0^\infty g(x\mu_u/\nu)\cdot p_{\boldsymbol{y}|u}(y(t)\mid x\mu_u/\nu\,;\,X,\Sigma_{\rm a})\cdot x^{\nu-1}\,\exp(-x)\,dx}{\int_0^\infty p_{\boldsymbol{y}|u}(y(t)\mid x\mu_u/\nu\,;\,X,\Sigma_{\rm a})\cdot x^{\nu-1}\,\exp(-x)\,dx}. \tag{8}$$

The integrals in the numerator and denominator of (8) are efficiently and accurately evaluated using the generalized Gauss-Laguerre quadrature formula (see [27, Ch. 5.3]):

$$\int_0^\infty f(x)\cdot x^{\nu-1}\exp(-x)\,dx \approx \sum_{l=1}^{L} w_l(\nu-1)\,f(x_l(\nu-1)), \tag{9}$$

where $f(x)$ is an arbitrary real function, L is the quadrature order, and $x_l(\nu-1)$ and $w_l(\nu-1)$, $l=1,2,\ldots,L$ are the abscissas and weights of the generalized Gauss-Laguerre quadrature with parameter $\nu-1$.

B. PX-EM Algorithm for Inverse Gamma Texture

We now propose a *complex multivariate t-distribution model* for the clutter and apply it to the measurement scenario in Section II. A similar clutter model was briefly discussed in [17, Sec. IV.B.3], where it was also referred to as the *generalized Cauchy distribution*. Assume that $w(t)=u(t)^{-1}$, $t=1,2,\ldots,N$ are gamma random variables with mean one and unknown shape parameter $\nu>0$. Consequently, $u(t)$ follows an *inverse gamma* distribution and the conditional distribution of $\boldsymbol{y}(t)$ given $w(t)$ is $p_{\boldsymbol{y}|u}(\boldsymbol{y}(t)|w(t)^{-1};X,\Sigma)$, see also (3). Integrating out the unobserved data $w(t)$, we obtain a *closed-form* expression for the marginal pdf of $\boldsymbol{y}(t)$:

$$p_{\boldsymbol{y}}(\boldsymbol{y}(t);X,\Sigma,\nu)=\frac{\Gamma\big(\nu+m\big)}{|\pi\Sigma|\cdot\Gamma\big(\nu\big)\cdot\nu^m}\cdot\Big\{1+[\boldsymbol{y}(t)-AX\boldsymbol{\phi}(t)]^H\,\Sigma^{-1}\,[\boldsymbol{y}(t)-AX\boldsymbol{\phi}(t)]/\nu\Big\}^{-\nu-m}, \tag{10}$$

which is the *complex multivariate t distribution* with location vector $AX\boldsymbol{\phi}(t)$, scale matrix Σ, and shape parameter ν. Here, the unknown parameters are $\boldsymbol{\theta}=\{X,\Sigma,\nu\}$. We first estimate X and Σ assuming that the shape parameter ν is *known* and then discuss the estimation of ν.

Known ν: For a fixed ν, we derive a PX-EM algorithm for estimating X and Σ by treating $w(t)$, $t=1,2,\ldots,N$ as the unobserved data and adding an auxiliary mean parameter for $w(t)$, similar to the gamma case discussed in Section III-A. The derivation of PX-EM algorithm is analogous to the one for gamma texture in Appendix A. Here, the resulting PX-EM algorithm consists of iterating between the following PX-E and PX-M steps:

PX-E Step: Compute

$$\widehat{w}^{(i)}(t)=(\nu+m)\cdot\Big\{\nu+[\boldsymbol{y}(t)-AX^{(i)}\boldsymbol{\phi}(t)]^H\cdot[\Sigma^{(i)}]^{-1}\,[\boldsymbol{y}(t)-AX^{(i)}\boldsymbol{\phi}(t)]\Big\}^{-1} \tag{11a}$$

for $t=1,2,\ldots,N$ and

$$T_1^{(i)} = \frac{1}{N}\cdot\sum_{t=1}^{N}\boldsymbol{y}(t)\boldsymbol{\phi}(t)^H\cdot\widehat{w}^{(i)}(t), \tag{11b}$$

$$T_2^{(i)} = \frac{1}{N}\cdot\sum_{t=1}^{N}\boldsymbol{y}(t)\boldsymbol{y}(t)^H\cdot\widehat{w}^{(i)}(t), \tag{11c}$$

$$T_3^{(i)} = \frac{1}{N}\cdot\sum_{t=1}^{N}\boldsymbol{\phi}(t)\boldsymbol{\phi}(t)^H\cdot\widehat{w}^{(i)}(t). \tag{11d}$$

PX-M Step: Compute

$$X^{(i+1)} = [A^H(S^{(i)})^{-1}A]^{-1}A^H(S^{(i)})^{-1}\,T_1^{(i)}(T_3^{(i)})^{-1}, \tag{12a}$$

$$\Sigma^{(i+1)} = \Big\{S^{(i)} + [I_m - Q^{(i)}(S^{(i)})^{-1}]\cdot T_1^{(i)}\,(T_3^{(i)})^{-1} \cdot (T_1^{(i)})^H\,[I_m - Q^{(i)}(S^{(i)})^{-1}]^H\Big\}\Big/\Big[\frac{1}{N}\sum_{t=1}^{N}\widehat{w}^{(i)}(t)\Big], \tag{12b}$$

where

$$S^{(i)} = T_2^{(i)} - T_1^{(i)}\,(T_3^{(i)})^{-1}\,(T_1^{(i)})^H, \tag{12c}$$

$$Q^{(i)} = A\,[A^H(S^{(i)})^{-1}A]^{-1}\,A^H. \tag{12d}$$

The above iteration is performed until $X^{(i)}$ and $\Sigma^{(i)}$ converge. Denote by $X^{(\infty)}(\nu)$ and $\Sigma^{(\infty)}(\nu)$ the estimates of X and Σ obtained upon convergence, where we emphasize their dependence on ν.

Unknown ν: We compute the ML estimate of ν by maximizing the observed-data log-likelihood function concentrated with respect to $\widehat{X}(\nu)$ and $\widehat{\Sigma}(\nu)$:

$$\widehat{\nu} = \arg\max_{\nu}\sum_{t=1}^{N}\ln p_{\boldsymbol{y}}(\boldsymbol{y}(t); X^{(\infty)}(\nu), \Sigma^{(\infty)}(\nu), \nu), \tag{13}$$

see also (10).

IV. Cramér-Rao Bound and Related Bounds

In this section, we first derive the CRB with general texture pdf assumption. Then we apply it for different texture distributions, see [28]. We also consider the hybrid CRB, which is not as tight as CRB.

A. General CRB Results

Denote by $p_u(u(t);\nu)$ the pdf of the texture $u(t)$. Then, according to the above measurement model, $\boldsymbol{y}(t)$ is a complex spherically invariant random vector (SIRV) with marginal pdf

$$p_{\boldsymbol{y}}(\boldsymbol{y}(t);\boldsymbol{\rho}) = \frac{1}{|\pi\Sigma|}\cdot g(\|\boldsymbol{z}(t;\boldsymbol{\xi},\boldsymbol{\eta})\|^2,\nu), \tag{14}$$

where

$$g(s,\nu) = \int_0^\infty \exp\Big(-\frac{s}{u}\Big)\cdot u^{-m}\cdot p_u(u;\nu)\;du, \tag{15a}$$

$$\boldsymbol{z}(t;\boldsymbol{\xi},\boldsymbol{\eta}) = \Sigma^{-1/2}\cdot[\boldsymbol{y}(t) - AX\phi(t)], \tag{15b}$$

and $\|\cdot\|$ denotes the Frobenius norm. Also, $\Sigma^{-1/2} = (\Sigma^{1/2})^{-1}$ where $\Sigma^{1/2}$ denotes a Hermitian square root of a Hermitian matrix Σ.

Given an arbitrary radius $\|\boldsymbol{z}(t;\boldsymbol{\xi},\boldsymbol{\eta})\| = r$, the concatenated vector of real and imaginary parts of $\boldsymbol{z}(t;\boldsymbol{\xi},\boldsymbol{\eta})$ is uniformly distributed on the surface of a $2m$-dimensional ball with radius r, centered at

the origin. Denote by g_1 and g_2 the partial derivatives of $g(\cdot,\cdot)$ with respect to its first and second entries, i.e. $g_1(s,\nu) = \partial g(s,\nu)/\partial s$ and $g_2(s,\nu) = \partial g(s,\nu)/\partial \nu$. For any well-behaved $g(\cdot,\cdot)$, changing the order of differentiation and integration leads to

$$g_1(s,\nu) = -\int_0^\infty \exp\Big(-\frac{s}{u}\Big)\cdot u^{-m-1}\cdot p_u(u;\nu)\ du \tag{16a}$$

$$g_2(s,\nu) = \int_0^\infty \exp\Big(-\frac{s}{u}\Big)\cdot u^{-m}\cdot \frac{\partial p_u(u;\nu)}{\partial \nu}\ du. \tag{16b}$$

Define the vector of signal and clutter parameters:

$$\boldsymbol{\rho} = [\boldsymbol{\xi}^T, \boldsymbol{\eta}^T, \nu]^T \tag{17a}$$

where the subscript "^{T}" denotes a transpose,

$$\boldsymbol{\xi} = [\mathrm{Re}\{\mathrm{vec}(X)\}^T, \mathrm{Im}\{\mathrm{vec}(X)\}^T]^T \tag{17b}$$

$$\boldsymbol{\eta} = [\mathrm{Re}\{\mathrm{vech}(\Sigma)\}^T, \mathrm{Im}\{\underline{\mathrm{vech}}(\Sigma)\}^T]^T \tag{17c}$$

and ν is the texture parameter[3]. Here, the vech and $\underline{\mathrm{vech}}$ operators create a single column vector by stacking elements below the main diagonal columnwise; vech includes the main diagonal, whereas $\underline{\mathrm{vech}}$ omits it. The Fisher information matrix (FIM) for $\boldsymbol{\rho}$ is computed by using [29, eqs. (3.21) and (3.23)]:

$$[\mathcal{I}]_{\rho_i\rho_k} = \mathrm{E}\Big\{\frac{\partial \ln p(\boldsymbol{y};\boldsymbol{\rho})}{\partial \rho_i}\frac{\partial \ln p(\boldsymbol{y};\boldsymbol{\rho})}{\partial \rho_k}\Big\} \tag{18a}$$

$$= -\mathrm{E}\Big\{\frac{\partial^2 \ln p(\boldsymbol{y};\boldsymbol{\rho})}{\partial \rho_i \partial \rho_k}\Big\} \tag{18b}$$

where $[\mathcal{I}]_{\rho_i\rho_k}$ denotes the FIM entry with respect to the parameters ρ_i and ρ_k, $i,k \in \{1,2,\ldots,\dim(\boldsymbol{\rho})\}$ and

$$\ln p(\boldsymbol{y};\boldsymbol{\rho}) = -N\ln|\pi\Sigma| + \sum_{t=1}^{N} \ln g(\|\boldsymbol{z}(t;\boldsymbol{\xi},\boldsymbol{\eta})\|^2, \nu) \tag{18c}$$

is the log-likelihood function. Then the CRB for $\boldsymbol{\rho}$ is

$$\mathrm{CRB} = \mathcal{I}^{-1}. \tag{18d}$$

To simplify the notation, we omit the dependencies of the FIM and CRB on the model parameters. We also omit details of the derivation and give the final FIM expressions (see Appendix B for details):

[3]We parameterize the texture pdf using only one parameter. The extension to multiple parameters is straightforward.

$$\mathcal{I}_{\xi_i\xi_k} = \frac{2\alpha_1}{m}\sum_{t=1}^{N}\mathrm{Re}\left[\phi^H(t)\frac{\partial X^H}{\partial \xi_k}A^H\ \Sigma^{-1}\ A\frac{\partial X}{\partial \xi_i}\phi(t)\right] \tag{19a}$$

$$\mathcal{I}_{\eta_i\eta_k} = N^2 c_{\eta_i\eta_k} + \frac{2N^2 c_{\eta_i\eta_k}}{m}\cdot\alpha_2 + \frac{N(N-1)c_{\eta_i\eta_k}}{m^2}\cdot\alpha_2^2 + \frac{N}{m(m+1)}\left[\,\mathrm{tr}(\Sigma^{-1}\frac{\partial\Sigma}{\partial\eta_i}\Sigma^{-1}\frac{\partial\Sigma}{\partial\eta_k}) + c_{\eta_i\eta_k}\right]\cdot\alpha_3 \tag{19b}$$

$$\mathcal{I}_{\nu\nu} = N\cdot\beta_1 \tag{19c}$$

$$\mathcal{I}_{\eta_i\nu} = \frac{N}{m}\,\mathrm{tr}\left(\Sigma^{-1}\frac{\partial\Sigma}{\partial\eta_i}\right)\cdot\beta_2 \tag{19d}$$

$$\mathcal{I}_{\xi_i\eta_k} = 0 \tag{19e}$$

$$\mathcal{I}_{\xi_i\nu} = 0 \tag{19f}$$

where

$$c_{\eta_i\eta_k} = \mathrm{tr}\left(\Sigma^{-1}\frac{\partial\Sigma}{\partial\eta_i}\right)\mathrm{tr}\left(\Sigma^{-1}\frac{\partial\Sigma}{\partial\eta_k}\right) \tag{20}$$

and

$$\alpha_1 = \frac{\int_0^\infty \frac{g_1^2(r^2,\nu)}{g(r^2,\nu)}\cdot r^{2m+1}\,dr}{\int_0^\infty g(r^2,\nu)\cdot r^{2m-1}\,dr} \tag{21a}$$

$$\alpha_2 = \frac{\int_0^\infty g_1^2(r^2,\nu)\cdot r^{2m+1}\,dr}{\int_0^\infty g(r^2,\nu)\cdot r^{2m-1}\,dr} \tag{21b}$$

$$\alpha_3 = \frac{\int_0^\infty \frac{g_1^2(r^2,\nu)}{g(r^2,\nu)}\cdot r^{2m+3}\,dr}{\int_0^\infty g(r^2,\nu)\cdot r^{2m-1}\,dr} \tag{21c}$$

$$\beta_1 = \frac{\int_0^\infty \left(\frac{g_2^2(r^2,\nu)}{g(r^2,\nu)} - \frac{\partial g_2(r^2,\nu)}{\partial\nu}\right)\cdot r^{2m-1}\,dr}{\int_0^\infty g(r^2,\nu)\cdot r^{2m-1}\,dr} \tag{21d}$$

$$\beta_2 = \frac{\int_0^\infty \left(\frac{\partial g_1(r^2,\nu)}{\partial\nu} - \frac{g_1(r^2,\nu)g_2(r^2,\nu)}{g(r^2,\nu)}\right)\cdot r^{2m+1}\,dr}{\int_0^\infty g(r^2,\nu)\cdot r^{2m-1}\,dr}. \tag{21e}$$

Here, (19a) and (19b) have been computed by using (18a) and the lemma, whereas (19c)-(19f) follow by using (18b).

Interestingly, the FIMs of compound-Gaussian models with different texture distributions share the common structure in (19a)-(19f) where the texture-specific quantities are the scalar coefficients in (21). The above FIM and CRB matrices are block-diagonal (see (19e) and (19f)), implying that the CRBs for the signal parameters $\boldsymbol{\xi}$ are uncoupled from the clutter parameters ν and $\boldsymbol{\eta}$. Hence, the CRB matrix for $\boldsymbol{\xi}$ remains the same whether or not ν and Σ are known. Similarly, the CRBs for $\boldsymbol{\eta}$ and ν remain the same whether or not X is known. Also, (19a) and (19b) simplify to the FIM expressions for complex Gaussian clutter when $\alpha_1 = m, \alpha_2 = -m$ and $\alpha_3 = m(m+1)$, see also [29, eq. (15.52)].

B. CRB for Specific Texture Distributions

Computing the texture-specific terms in (21) typically involves two-dimensional integration that cannot be evaluated in closed form. This integration can be performed using Gauss quadratures, see

e.g. [27, Ch. 5.3]. Here we use the gamma texture as an example.

Gamma texture: Here we use the same model as in Section III-A. After applying a change-of-variable transformation $x = \nu u$ in (15a) and (16), we evaluate both integrals in (21) using the generalized Gauss-Laguerre quadrature formula (see (9).) For example, the formula used to compute α_1 is given in (22) where, to simplify the notation, we omit the dependencies of the abscissas and weights on $\nu - 1$.

$$\alpha_1 = \frac{\sum_{l_1=1}^{L} \frac{\left(\sum_{l_2=1}^{L} \exp(-\frac{\nu x_{l_1}^2}{x_{l_2}}) \nu x_{l_2}^{-(m+1)} \cdot w_{l_2}\right)^2}{\sum_{l_3=1}^{L} \exp(-\frac{\nu x_{l_1}^2}{x_{l_3}}) x_{l_3}^{-m} \cdot w_{l_3}} \exp(x_{l_1}) \cdot w_{l_1}}{\sum_{l_4=1}^{L} \left(\sum_{l_5=1}^{L} \exp(-\frac{\nu x_{l_4}^2}{x_{l_5}}) x_{l_5}^{-m} \cdot w_{l_5}\right) \exp(x_{l_4}) \cdot w_{l_4}}. \tag{22}$$

In Appendix C, we derive other coefficients for gamma-distributed texture.

Inverse-gamma texture: We use the model discussed in Section III-B. In this case, (15a) and (16) can be evaluated in closed form, leading to the following simple expressions for the texture-specific terms in (21a)-(21e) (see Appendix C):

$$\alpha_1 = \frac{m(\nu+m)}{\nu+m+1} \tag{23a}$$

$$\alpha_2 = -m \tag{23b}$$

$$\alpha_3 = \frac{m(m+1)(\nu+m)}{\nu+m+1} \tag{23c}$$

$$\beta_1 = \mathrm{TG}(\nu) - \mathrm{TG}(\nu+m) - \frac{m(\nu+m+2)}{\nu(\nu+m)(\nu+m+1)} \tag{23d}$$

$$\beta_2 = -\frac{m}{(\nu+m)(\nu+m+1)} \tag{23e}$$

where $\mathrm{TG}(x) = d^2[\ln \Gamma(x)]/dx^2$ is the trigamma function. Interestingly, the CRB matrix for the signal parameters $\boldsymbol{\xi}$ is proportional to the corresponding CRB matrix for complex Gaussian clutter, with the proportionality factor $(\nu+m+1)/(\nu+m)$ always greater than one.

As $\nu \to \infty$, the inverse gamma texture distribution degenerates to a constant, the marginal pdf of $\boldsymbol{y}(t)$ in (14) reduces to the complex Gaussian distribution in (3) with $u(t) \equiv 1$, and (19a) and (19b) simplify to the FIM expressions for complex Gaussian clutter.

C. Hybrid CRB (HCRB)

The CRB is a lower bound of the covariance of all unbiased estimators of an unknown parameter vector. However, in some scenarios, we need to assess the estimation performance quickly but not so tightly. Thus we also consider the computation of a less optimal bound, the HCRB.

The HCRB is defined in [30]:

$$[I(\boldsymbol{\Theta})]_{ij} = \mathrm{E}_u\Big\{\mathrm{E}_{\boldsymbol{y}|u}\{\frac{\partial \ln p_{\boldsymbol{y},u}(\boldsymbol{y},u;\boldsymbol{\Theta})}{\partial\theta_i}\frac{\partial \ln p_{\boldsymbol{y},u}(\boldsymbol{y},u;\boldsymbol{\Theta})}{\partial\theta_j}\}\Big\} \tag{24a}$$

$$\mathrm{HCRB}(\theta_i) = [I^{-1}(\boldsymbol{\Theta})]_{ii} \tag{24b}$$

Note that the HCRB takes the expectation over the unobserved data $u(t)$ for the whole product of two complete data score functions while the CRB takes the expectations respectively. This usually reduces the calculation effort at the cost of degraded bound tightness. Similarly, we omit the dependencies of the information matrix and HCRB on the model parameters. With the derivation presented in Appendix D, the information entries of the HCRB for general texture are

$$I_{\xi_i\xi_j} = 2\sum_{t=1}^{N} \mathrm{Re}\Big[\mathrm{tr}(A\frac{\partial X}{\partial \xi_i}\phi(t)\cdot\phi^H(t)\frac{\partial X^H}{\partial \xi_i}A^H\Sigma^{-1})\Big]\cdot \mathrm{E}_u\{u^{-1}(t)\} \tag{25a}$$

$$I_{\eta_i\eta_j} = \frac{N(m+2)}{(m+1)}\,\mathrm{tr}(\Sigma^{-1}\frac{\partial\Sigma}{\partial\eta_i}\Sigma^{-1}\frac{\partial\Sigma}{\partial\eta_j}) \tag{25b}$$

$$I_{\nu\nu} = -\sum_{t=1}^{N}\mathrm{E}_u\Big\{\frac{1}{p_u}\frac{\partial^2 p_u}{\partial\nu^2} - \frac{1}{p_u^2}\Big(\frac{\partial p_u}{\partial\nu}\Big)^2\Big\} \tag{25c}$$

$$I_{\eta_i\nu} = I_{\xi_i\nu} = I_{\eta_i\xi_j} = 0 \tag{25d}$$

Compared with FIM, the information matrix of HCRB is much simpler and easier to compute. It is interesting to observe that

- $\boldsymbol{\xi}, \boldsymbol{\eta}$ and ν are decoupled from each other. The HCRB is a block diagonal matrix with three blocks. Note that in the CRB, $\boldsymbol{\eta}$ and ν are coupled.
- $I_{\eta_i\eta_j}$ is constant. It does not change over the choice of texture models.
- $u(t)$ affects $I_{\xi_i\xi_j}$ in a simple way – by multiplying a constant with $\mathrm{E}_u(u^{-1}(t))$.

V. Numerical Examples

The numerical examples presented here assess the estimation accuracy of the ML estimates of X, Σ, and the shape parameters of the texture components. We consider a measurement scenario with a 3-element radar array and $P = 3$ pulses, implying that $m = 9$. We select a rank-one target scenario with $\boldsymbol{\phi}(t) = 1$, $t = 1, 2, \ldots, N$, complex target amplitude $X = 0.207\cdot\exp(j\pi/7)$, and

$$A = \boldsymbol{b}(\varpi)\otimes\boldsymbol{a}(\vartheta), \tag{26}$$

where $\boldsymbol{b}(\varpi) = [1, \exp(j2\pi\varpi), \exp(j4\pi\varpi)]^T$ with *normalized Doppler frequency* $\varpi = 0.42$, and $\boldsymbol{a}(\vartheta) = [1, \exp(j2\pi\vartheta), \exp(j4\pi\vartheta)]^T$ with *spatial frequency* $\vartheta = 0.926$. Here, $\otimes$ denotes the Kronecker product. The speckle covariance matrix Σ was generated using a model similar to that in [31, Sec. 2.6] with 1000 patches. The (p, q)th element of the covariance matrix of the speckle component was chosen as

$$\Sigma_{p,q} = \sigma^2\cdot 0.9^{|p-q|}\cdot\exp[j(\pi/2)(p-q)], \tag{27}$$

which is the correlated noise covariance model used in [33] (see also references therein). In the simulations presented here, we select $\sigma^2 = 10.17$. The order of the Gauss-Hermite and generalized Gauss-Laguerre quadratures was $L = 50$.

We compare the average mean-square errors (MSEs) of the ML estimates of $\boldsymbol{\xi}, \boldsymbol{\eta}$ and ν over 2000 independent trials with the corresponding CRBs derived in Section IV. We also show the HCRBs in the results. Note: we just shown the average of elements of $\boldsymbol{\xi}, \boldsymbol{\eta}$, and ν in this paper.

First we study the performance of the ML estimation for gamma texture in Section III-A. We have set the shape parameter to $\nu = 2$. The Fig. 1 shows the MSEs for the ML estimates of X and ν and the average MSE for the ML estimates of the speckle covariance parameters as functions of N.

In Fig. 2, we show the performance of the ML estimation for the inverse gamma texture in Section III-A. Here, the shape parameter was set to $\nu = 4$. Fig. 2 shows the MSEs for the ML estimates of X and ν and the average MSE for the ML estimates of the speckle covariance parameters as functions of N.

In Fig. 1 and Fig. 2, the MSEs matches the CRBs very well when the number of observations increases, which indicates that the PX-EM is the optimal asymptotically efficient estimation for target and the clutter parameters. HCRBs show their loose estimation to the lower bound of estimation variance as mentioned before. The average signal power and clutter power can be calculated by their definitions:

$$P_{\mathrm{s}} = \mathrm{E}\left\{[AX\boldsymbol{\phi}(t)]^H \cdot [AX\boldsymbol{\phi}(t)]\right\}, \tag{28a}$$

$$P_{\mathrm{c}} = \mathrm{E}\left\{\boldsymbol{e}(t)^H\boldsymbol{e}(t)\right\} = \mathrm{E}\left\{\mathrm{tr}[\boldsymbol{e}(t)\boldsymbol{e}(t)^H]\right\} = \mathrm{E}\left\{u(t)\right\} \cdot \mathrm{tr}(\Sigma). \tag{28b}$$

Thus the signal-to-noise ratio (SNR) in the above examples are -6.70 dB and -7.95 dB respectively. Note that in these examples, the SNRs do not change with number of snapshots N.

We also investigate the performance of the clutter spikiness, which can be indicated by the clutter texture parameter ν. In Fig. 3, we show the average MSEs of the estimates under the inverse-gamma texture model for four different ν values. The results are the averaged MSEs among 500 independent trials. When ν decreases, i.e., the clutter becomes spikier, the results show that there is no much difference for the performance of estimate of X, while the estimate for Σ becomes worse and the estimate for ν becomes more accurate.

VI. Concluding Remarks

In this paper, we developed maximum likelihood algorithms for estimating the parameters of a target with compound-Gaussian distributed clutter. The algorithms are potentially useful to mitigate sea-clutter in high-resolution and low-grazing-angle radar. The proposed maximum likelihood estimation is based on the parameter-expanded expectation-maximization algorithm. We also computed the Cramér-Rao bounds and their hybrid versions for the unknown parameters. Our results are based on the general compound-Gaussian model and can be applied to various texture distributions. We obtained compact

closed-form results of the bounds for the inverse-gamma texture. Numerical simulations confirmed the asymptotic efficiency of our estimates.

APPENDIX A
PX-EM ALGORITHM DERIVATION FOR GAMMA TEXTURE

We derive the PX-EM algorithm to estimate the parameter set $\boldsymbol{\theta} = \{X, \Sigma, \nu\}$ given the observations $\boldsymbol{y}$.

With the auxiliary parameter μ_u, the augmented parameter set is $\boldsymbol{\theta}_{\rm a} = \{X, \Sigma_{\rm a}, \nu, \mu_u\}$, and the augmented model can be written as:

$$\boldsymbol{y}(t)\big|u(t) \;\sim\; \mathcal{CN}(AX\phi(t), u(t)\Sigma_{\rm a}), \tag{A.29a}$$

$$u(t) \;\sim\; \mathrm{Gamma}(\mu_u, \nu). \tag{A.29b}$$

Denote $\boldsymbol{u} = [u(1), u(2), \ldots, u(N)]^T$. Instead of maximizing the intractable likelihood function for the measurement $\boldsymbol{y}(t)$, we maximize the *complete data log-likelihood*:

$$L_{\rm c}(\boldsymbol{y}, \boldsymbol{u}; \boldsymbol{\theta}_{\rm a}) = \sum_{t=1}^{N} \ln p_{\boldsymbol{y}|u}(\boldsymbol{y}(t)|u(t); X, \Sigma_{\rm a}) + \sum_{t=1}^{N} \ln p_u(u(t); \nu, \mu_u). \tag{A.30}$$

Substitute (3) and (5) into (A.30), we can write the complete data log-likelihood as:

$$\begin{aligned} L_{\rm c} \;=\; & -Nm\,\tau_4(\boldsymbol{y}, \boldsymbol{u}) - N\,\mathrm{tr}[\mathcal{T}_2(\boldsymbol{y}, \boldsymbol{u}) \cdot \Sigma_{\rm a}^{-1}] - N\,\mathrm{tr}[X^H A^H \Sigma_{\rm a}^{-1} AX \cdot \mathcal{T}_3(\boldsymbol{y}, \boldsymbol{u})] \\ & + N\,\mathrm{tr}[X^H A^H \Sigma_{\rm a}^{-1} \cdot \mathcal{T}_1(\boldsymbol{y}, \boldsymbol{u})] + N\,\mathrm{tr}[\mathcal{T}_1(\boldsymbol{y}, \boldsymbol{u})^H \cdot \Sigma_{\rm a}^{-1} AX] - \frac{N\nu}{\mu_u}\tau_5(\boldsymbol{y}, \boldsymbol{u}) \\ & + (\nu - 1)\tau_4(\boldsymbol{y}, \boldsymbol{u}) - N\nu \ln \mu_u + N \ln\left[\frac{\nu^\nu}{\Gamma(\nu)}\right] - Nm \ln \pi \end{aligned} \tag{A.31a}$$

where $\mathcal{T}_1(\boldsymbol{y}, \boldsymbol{u}), \mathcal{T}_2(\boldsymbol{y}, \boldsymbol{u}), \mathcal{T}_3(\boldsymbol{y}, \boldsymbol{u}), \tau_4(\boldsymbol{y}, \boldsymbol{u}), \tau_5(\boldsymbol{y}, \boldsymbol{u})$ are *natural complete-data sufficient statistics* [25, ch.1.6.2]:

$$\mathcal{T}_1(\boldsymbol{y}, \boldsymbol{u}) \;=\; \frac{1}{N} \cdot \sum_{t=1}^{N} \boldsymbol{y}(t)\boldsymbol{\phi}(t)^H \cdot u(t)^{-1}, \tag{A.32a}$$

$$\mathcal{T}_2(\boldsymbol{y}, \boldsymbol{u}) \;=\; \frac{1}{N} \cdot \sum_{t=1}^{N} \boldsymbol{y}(t)\boldsymbol{y}(t)^H \cdot u(t)^{-1}, \tag{A.32b}$$

$$\mathcal{T}_3(\boldsymbol{y}, \boldsymbol{u}) \;=\; \frac{1}{N} \cdot \sum_{t=1}^{N} \boldsymbol{\phi}(t)\boldsymbol{\phi}(t)^H \cdot u(t)^{-1}, \tag{A.32c}$$

$$\tau_4(\boldsymbol{y}, \boldsymbol{u}) \;=\; \frac{1}{N} \cdot \sum_{t=1}^{N} \ln u(t), \tag{A.32d}$$

$$\tau_5(\boldsymbol{y}, \boldsymbol{u}) \;=\; \frac{1}{N} \cdot \sum_{t=1}^{N} u(t), \tag{A.32e}$$

We first assume that ν is a known constant. Take derivative of (A.31a) with respect to X, $\Sigma_{\rm a}$, μ_u respectively and let these derivatives equal to zero, we get a set of equations. Solving these equations, we can obtain the ML estimates of X, $\Sigma_{\rm a}$, μ_u (see [12] for the derivations of the ML estimates for

X and $\Sigma_{\rm a}$):

$$\widehat{X} = [A^H S^{-1} A]^{-1} A^H S^{-1} \cdot \mathcal{T}_1(\boldsymbol{y}, \boldsymbol{u})\, \mathcal{T}_3(\boldsymbol{y}, \boldsymbol{u})^{-1}, \tag{A.33a}$$

$$\widehat{\Sigma}_{\rm a} = S + [I_m - QS^{-1}]\, \mathcal{T}_1(\boldsymbol{y}, \boldsymbol{u}) \cdot \mathcal{T}_3(\boldsymbol{y}, \boldsymbol{u})^{-1} \mathcal{T}_1(\boldsymbol{y}, \boldsymbol{u})^H\, [I_m - QS^{-1}]^H, \tag{A.33b}$$

$$\widehat{\mu}_u = \tau_5(\boldsymbol{y}, \boldsymbol{u}), \tag{A.33c}$$

$$\widehat{\Sigma} = \widehat{\mu}_u \cdot \widehat{\Sigma}_{\rm a}, \tag{A.33d}$$

where

$$S = \mathcal{T}_2(\boldsymbol{y}, \boldsymbol{u}) - \mathcal{T}_1(\boldsymbol{y}, \boldsymbol{u}) \cdot \mathcal{T}_3(\boldsymbol{y}; \boldsymbol{u})^{-1} \cdot \mathcal{T}_1(\boldsymbol{y}, \boldsymbol{u})^H, \tag{A.33e}$$

$$Q = A\, [A^H S^{-1} A]^{-1} A^H, \tag{A.33f}$$

With these estimates, we can find the ML estimate of ν that maximizes the concentrated complete data log-likelihood:

$$\widehat{\nu} = \arg\max_{\nu} \Big\{ -\ln\Gamma(\nu) + \nu \ln \nu - \nu \ln[\tau_5(\boldsymbol{y}, \boldsymbol{u})] + \nu \tau_4(\boldsymbol{y}, \boldsymbol{u}) - \nu \Big\}.$$

In the PX-E step, we calculate conditional expectations $\mathrm{E}_{u|\boldsymbol{y}}[\cdot]$ of sufficient statistics $\mathcal{T}_1(\boldsymbol{y}, \boldsymbol{u})$, $\mathcal{T}_2(\boldsymbol{y}, \boldsymbol{u})$, $\mathcal{T}_3(\boldsymbol{y}, \boldsymbol{u})$, $\tau_4(\boldsymbol{y}, \boldsymbol{u})$, $\tau_5(\boldsymbol{y}, \boldsymbol{u})$ (see (6a)-(6e)). Then in the PX-M step, we use these expectations to calculate the ML estimates of parameters in $\boldsymbol{\theta}_{\rm a}$. The iteration goes between PX-E and PX-M steps until estimation results converges.

APPENDIX B
DERIVATION OF THE SCORE FUNCTIONS AND FISHER INFORMATION MATRIX (FIM)

K.L. Lange *et al* derived the FIM of multivariate real t-distribution in Appendix B of [19]. Here we follow the same procedure to derive the entries of the FIM of complex compound-Gaussian distribution.

Before starting to derive the FIM entries, we list some preliminary results that will be used in the derivation here.

Lemma 1: For $\boldsymbol{z} \in \mathbb{R}^k$ uniformly distributed on real sphere $\|\boldsymbol{z}\| = r$ and any $k \times k$ real matrices A and B,

$$\mathrm{E}\Big(\frac{\boldsymbol{z}^H}{\|\boldsymbol{z}\|} A \frac{\boldsymbol{z}}{\|\boldsymbol{z}\|} \Big| \|\boldsymbol{z}\| \Big) = \frac{1}{k} \operatorname{tr}(A), \tag{B.34}$$

$$\mathrm{E}\Big(\frac{\boldsymbol{z}^H}{\|\boldsymbol{z}\|} A \frac{\boldsymbol{z}}{\|\boldsymbol{z}\|} \frac{\boldsymbol{z}^H}{\|\boldsymbol{z}\|} B \frac{\boldsymbol{z}}{\|\boldsymbol{z}\|} \Big| \|\boldsymbol{z}\| \Big) = \frac{1}{k(k+2)} [2 \operatorname{tr}(AB) + \operatorname{tr}(A) \operatorname{tr}(B)]. \tag{B.35}$$

Proof. See [19] Appendix B.

Lemma 2: For $\boldsymbol{z} \in \mathbb{C}^k$ uniformly distributed on sphere $\|\boldsymbol{z}\| = r$ and any $k \times k$ matrices A and B,

$$\mathrm{E}\Big(\frac{\boldsymbol{z}^H}{\|\boldsymbol{z}\|} A \frac{\boldsymbol{z}}{\|\boldsymbol{z}\|}\Big|\|\boldsymbol{z}\|\Big) = \frac{1}{k}\operatorname{tr}(A), \tag{B.36}$$

$$\mathrm{E}\Big(\frac{\boldsymbol{z}^H}{\|\boldsymbol{z}\|} A \frac{\boldsymbol{z}}{\|\boldsymbol{z}\|} \frac{\boldsymbol{z}^H}{\|\boldsymbol{z}\|} B \frac{\boldsymbol{z}}{\|\boldsymbol{z}\|}\Big|\|\boldsymbol{z}\|\Big) = \frac{1}{k(k+1)}[\operatorname{tr}(AB) + \operatorname{tr}(A)\operatorname{tr}(B)]. \tag{B.37}$$

Proof: let $\boldsymbol{z} = \boldsymbol{z}_{\mathrm{R}} + i\boldsymbol{z}_{\mathrm{I}}$, where $\boldsymbol{z}_{\mathrm{R}}$ and $\boldsymbol{z}_{\mathrm{I}}$ are real and imaginary parts of vector $\boldsymbol{z}$. By applying Lemma 1, the proof is trivial.

Lemma 3: For $\boldsymbol{z}_1, \boldsymbol{z}_2 \in \mathbb{C}^k$ independently uniformly distributed on sphere $\|\boldsymbol{z}\| = r$ and any $k \times k$ matrices A and B,

$$\mathrm{E}\Big(\frac{\boldsymbol{z}_1^H}{\|\boldsymbol{z}_1\|} A \frac{\boldsymbol{z}_2}{\|\boldsymbol{z}_2\|}\Big|\|\boldsymbol{z}_1\|, \|\boldsymbol{z}_2\|\Big) = 0, \tag{B.38}$$

$$\mathrm{E}\Big(\frac{\boldsymbol{z}_1^H}{\|\boldsymbol{z}_1\|} A \frac{\boldsymbol{z}_1}{\|\boldsymbol{z}_1\|} \frac{\boldsymbol{z}_2^H}{\|\boldsymbol{z}_2\|} B \frac{\boldsymbol{z}_2}{\|\boldsymbol{z}_2\|}\Big|\|\boldsymbol{z}_1\|, \|\boldsymbol{z}_2\|\Big) = \frac{1}{k^2}\operatorname{tr}(A)\operatorname{tr}(B). \tag{B.39}$$

Proof: Note that $\boldsymbol{z}_1$ and $\boldsymbol{z}_2$ are independent,

$$\mathrm{E}\Big(\frac{\boldsymbol{z}_1^H}{\|\boldsymbol{z}_1\|} A \frac{\boldsymbol{z}_2}{\|\boldsymbol{z}_2\|}\Big|\|\boldsymbol{z}_1\|, \|\boldsymbol{z}_2\|\Big) = \mathrm{E}\Big(\frac{\boldsymbol{z}_1^H}{\|\boldsymbol{z}_1\|}\Big|\|\boldsymbol{z}_1\|\Big) \cdot A \cdot \mathrm{E}\Big(\frac{\boldsymbol{z}_2}{\|\boldsymbol{z}_2\|}\Big|\|\boldsymbol{z}_2\|\Big).$$

By symmetry,

$$\mathrm{E}\Big(\frac{\boldsymbol{z}_1}{\|\boldsymbol{z}_1\|}\Big|\|\boldsymbol{z}_1\|\Big) = \mathrm{E}\Big(\frac{\boldsymbol{z}_2}{\|\boldsymbol{z}_2\|}\Big|\|\boldsymbol{z}_2\|\Big) = 0.$$

The first equation is proved. By applying the first equation in Lemma 2, the second equation is also easily proved.

Now we start the derivation of FIM. First, recall the complete data log-likelihood (18c). We can get the contribution of each parameter to the score vector through straightforward calculations:

$$\frac{\partial \mathcal{L}}{\partial \xi_i} = -\sum_{t=1}^{N} \frac{g_1(\|\boldsymbol{z}(t)\|^2, \nu)}{g(\|\boldsymbol{z}(t)\|^2, \nu)} \cdot \Big[\boldsymbol{z}^H(t)\Sigma^{-\frac{1}{2}} A \frac{\partial X}{\partial \xi_i}\phi(t) + \phi^H(t)\frac{\partial X^H}{\partial \xi_i} A^H \Sigma^{-\frac{1}{2}}\boldsymbol{z}(t)\Big], \tag{B.40a}$$

$$\frac{\partial \mathcal{L}}{\partial \eta_i} = -N \cdot \operatorname{tr}(\Sigma \frac{\partial \Sigma}{\partial \eta_i}) - \sum_{t=1}^{N} \frac{g_1(\|\boldsymbol{z}(t)\|^2, \nu)}{g(\|\boldsymbol{z}(t)\|^2, \nu)} \cdot \big[\boldsymbol{z}^H(t)\Sigma^{-\frac{1}{2}} \frac{\partial \Sigma}{\partial \eta_i}\Sigma^{-\frac{1}{2}}\boldsymbol{z}(t)\big], \tag{B.40b}$$

$$\frac{\partial \mathcal{L}}{\partial \nu} = \sum_{t=1}^{N} \frac{g_2(\|\boldsymbol{z}(t)\|^2, \nu)}{g(\|\boldsymbol{z}(t)\|^2, \nu)}. \tag{B.40c}$$

These rules are used in the derivation:

$$\frac{\partial}{\partial \xi_i}[(\boldsymbol{y}-\boldsymbol{\mu})^H \Sigma^{-1}(\boldsymbol{y}-\boldsymbol{\mu})] = -\Big[\frac{\partial \boldsymbol{\mu}^H}{\partial \xi_i}\Sigma^{-1}(\boldsymbol{y}-\boldsymbol{\mu}) + (\boldsymbol{y}-\boldsymbol{\mu})^H \Sigma^{-1}\frac{\partial \boldsymbol{\mu}}{\partial \xi_i}\Big],$$

$$\frac{\partial}{\partial \eta_i}\ln|\Sigma| = \operatorname{tr}\Big(\Sigma^{-1}\frac{\partial \Sigma}{\partial \eta_i}\Big),$$

and

$$\frac{\partial \Sigma^{-1}}{\partial \eta_i} = -\Sigma^{-1}\frac{\partial \Sigma}{\partial \eta_i}\Sigma^{-1}.$$

The entry of FIM corresponding to X is

$$\begin{aligned}\mathcal{I}_{\xi_i\xi_j} &= \mathrm{E}\Big\{\frac{\partial \mathcal{L}}{\partial \xi_i}\frac{\partial \mathcal{L}}{\partial \xi_j}\Big\} \\ &= \frac{2}{m}\cdot \mathrm{E}\Big((\frac{g_1(\|\boldsymbol{z}(t)\|^2,\nu)}{g(\|\boldsymbol{z}(t)\|^2,\nu)}\|\boldsymbol{z}(t)\|^2\Big)\cdot\sum_{t=1}^{N}\mathrm{Re}\Big\{\mathrm{tr}\Big(A\frac{\partial X}{\partial \xi_i}\phi(t)\ \ \phi^H(t)\frac{\partial X^H}{\partial \xi_j}A^H\Sigma^{-1}\Big)\Big\} \qquad \text{(B.41a)}\end{aligned}$$

Using Lemma 2 and Lemma 3, we can get the following results:

$$\begin{aligned}\mathcal{I}_{\eta_i\eta_j} &= \mathrm{E}\Big\{\frac{\partial \mathcal{L}}{\partial \eta_i}\frac{\partial \mathcal{L}}{\partial \eta_j}\Big\} \\ &= N^2 c_{\eta_i\eta_j} + \frac{2Nc_{\eta_i\eta_j}}{m}\cdot\sum_{t=1}^{N}\mathrm{E}\Big\{\frac{g_1(\|\boldsymbol{z}(t)\|^2,\nu)}{g(\|\boldsymbol{z}(t)\|^2,\nu)}\cdot\|\boldsymbol{z}(t)\|^2\Big\} \\ &\quad + \frac{1}{m(m+1)}[\mathrm{tr}(\Sigma^{-1}\frac{\partial\Sigma}{\partial\eta_i}\Sigma^{-1}\frac{\partial\Sigma}{\partial\eta_j}) + c_{\eta_i\eta_j}]\cdot\sum_{t=1}^{N}\mathrm{E}\Big\{\Big(\frac{g_1(\|\boldsymbol{z}(t)\|^2,\nu)}{g(\|\boldsymbol{z}(t)\|^2,\nu)}\Big)^2\|\boldsymbol{z}(t)\|^4\Big\} \\ &\quad + \frac{N(N-1)c_{\eta_i\eta_j}}{m^2}\cdot\mathrm{E}^2\Big\{\frac{g_1(\|\boldsymbol{z}(t)\|^2,\nu)}{g(\|\boldsymbol{z}(t)\|^2,\nu)}\cdot\|\boldsymbol{z}(t)\|^2\Big\}, \qquad \text{(B.42a)}\end{aligned}$$

where $c_{\eta_i\eta_j} = \mathrm{tr}(\Sigma^{-1}\frac{\partial\Sigma}{\partial\eta_i})\,\mathrm{tr}(\Sigma^{-1}\frac{\partial\Sigma}{\partial\eta_j})$. See [32] for details.

The entry of the FIM matrix related to ν can be derived directly:

$$\mathcal{I}_{\nu\nu} = \mathrm{E}\Big\{-\frac{\partial^2\mathcal{L}}{\partial\nu^2}\Big\} = -N\mathrm{E}\Big\{\frac{\frac{\partial g_2(\|\boldsymbol{z}(t)\|^2,\nu)}{\partial\nu}}{g(\|\boldsymbol{z}(t)\|^2,\nu)} - \Big(\frac{g_2(\|\boldsymbol{z}(t)\|^2,\nu)}{g(\|\boldsymbol{z}(t)\|^2,\nu)}\Big)^2\Big\}. \qquad \text{(B.43)}$$

Also,

$$\begin{aligned}I_{\eta_i\nu} &= \mathrm{E}\Big\{-\frac{\partial^2\mathcal{L}}{\partial\eta_i\partial\nu}\Big\} \\ &= \mathrm{E}\Big\{\sum_{t=1}^{N}\frac{\frac{\partial g_1(\|\boldsymbol{z}(t)\|^2,\nu)}{\partial\nu}g(\|\boldsymbol{z}(t)\|^2,\nu) - g_1(\|\boldsymbol{z}(t)\|^2,\nu)g_2(\|\boldsymbol{z}(t)\|^2,\nu)}{g^2(\|\boldsymbol{z}(t)\|^2,\nu)}\big[\boldsymbol{z}^H(t)\Sigma^{-\frac{1}{2}}\frac{\partial\Sigma}{\partial\eta_i}\Sigma^{-\frac{1}{2}}\boldsymbol{z}(t)\big]\Big\} \\ &= \frac{1}{m}\,\mathrm{tr}\Big(\Sigma^{-1}\frac{\partial\Sigma}{\partial\eta_i}\Big)\cdot\sum_{t=1}^{N}\mathrm{E}\Big\{\frac{\frac{\partial g_1(\|\boldsymbol{z}(t)\|^2,\nu)}{\partial\nu}g(\|\boldsymbol{z}(t)\|^2,\nu) - g_1(\|\boldsymbol{z}(t)\|^2,\nu)g_2(\|\boldsymbol{z}(t)\|^2,\nu)}{g^2(\|\boldsymbol{z}(t)\|^2,\nu)}\|\boldsymbol{z}(t)\|^2\Big\}\end{aligned}$$

(B.44a)

Finally we prove that

$$\mathcal{I}_{\xi_i\eta_j} = 0 \qquad \text{(B.45)}$$

and

$$\mathcal{I}_{\xi_i\nu} = 0 \qquad \text{(B.46)}$$

Proof: Since $\mathcal{I}_{\xi_i\eta_j} = \mathrm{E}\,\{\frac{\partial\mathcal{L}}{\partial\xi_i}\frac{\partial\mathcal{L}}{\partial\eta_j}\}$ and $\mathcal{I}_{\xi_i\nu} = \mathrm{E}\,\{\frac{\partial\mathcal{L}}{\partial\xi_i}\frac{\partial\mathcal{L}}{\partial\nu}\}$, for fixed $\|\boldsymbol{z}\|$, $\frac{\partial\mathcal{L}}{\partial\xi_i}$ is an odd function of $\boldsymbol{z}$ (B.40a) while $\frac{\partial\mathcal{L}}{\partial\eta_i}$ and $\frac{\partial\mathcal{L}}{\partial\nu}$ are even functions of $\boldsymbol{z}$ (B.40b).

APPENDIX C
CALCULATION OF EXPECTATIONS

In this section, we propose the calculation method of expectations derived in Appendix A. First recall that for any well-behaved function $f(r)$ and SIRV real vector $\boldsymbol{w} \in \mathbb{R}^k$ with pdf in the form of $|\pi\Sigma|^{-1/2}\, g(\|\boldsymbol{w}\|^2, \nu)$,

$$\mathrm{E}\left(f(\|\boldsymbol{w}\|)\right) = \int_0^\infty f(r) g(r^2, \nu) r^{k-1} c_k \; dr, \tag{C.47}$$

where c_k is the surface area of the unit sphere in $\mathbb{R}^k$. See [19], Appendix A.

Now build a 1-1 map $\mathbb{C}^m : \boldsymbol{z} \to \mathbb{R}^{2m} : \boldsymbol{w}$ by letting $\boldsymbol{w} = [\boldsymbol{z}_{\mathrm{R}}^T, \boldsymbol{z}_{\mathrm{I}}^T]^T$, where $\boldsymbol{z}_{\mathrm{R}}$ and $\boldsymbol{z}_{\mathrm{I}}$ are the real and imaginary parts of $\boldsymbol{z}$ respectively. Clearly, if $\boldsymbol{z}$ is SIRV in $\mathbb{C}^m$, $\boldsymbol{w}$ will be SIRV in $\mathbb{R}^{2m}$. Also note that $\|\boldsymbol{z}\| = \|\boldsymbol{w}\|$, where $\|\cdot\|$ denotes the L^2 norm. Applying (C.47), we get

$$\mathrm{E}\left(f(\|\boldsymbol{z}\|)\right) = \mathrm{E}\left(f(\|\boldsymbol{w}\|)\right) = \int_0^\infty f(r) g(r^2, \nu) r^{2m-1} c_{2m} \; dr. \tag{C.48}$$

Since $\mathrm{E}\left(1\right) = 1$, we can get following result

$$c_{2m} = \frac{1}{\int_0^\infty g(r^2, \nu) r^{2m-1}\, dr}. \tag{C.49}$$

Define

$$\alpha_1 = \mathrm{E}\left\{ \left(\frac{g_1(\|\boldsymbol{z}(t)\|^2, \nu)}{g(\|\boldsymbol{z}(t)\|^2, \nu)} \|\boldsymbol{z}(t)\|^2 \right\}. \right. \tag{C.50}$$

By applying (C.48) and (C.49),

$$\begin{aligned} \alpha_1 &= \int_0^\infty \left(\frac{g_1(r^2, \nu)}{g(r^2, \nu)} \right)^2 r^2 g(r^2, \nu) \cdot r^{2m-1} c_{2m} \; dr \\ &= \frac{\int_0^\infty \frac{g_1^2(r^2, \nu)}{g(r^2, \nu)} \cdot r^{2m+1} \; dr}{\int_0^\infty g(r^2, \nu) \cdot r^{2m-1} \; dr} \end{aligned}$$

Similarly,

$$\begin{aligned}
\alpha_2 &= \mathrm{E}\Big\{\frac{g_1(\|\boldsymbol{z}(t)\|^2,\nu)}{g(\|\boldsymbol{z}(t)\|^2,\nu)}\|\boldsymbol{z}(t)\|^2\Big\} \\
&= \int_0^\infty \frac{g_1(r^2,\nu)}{g(r^2,\nu)} r^2 g(r^2,\nu)\cdot r^{2m-1}c_{2m}\ dr \\
&= \frac{\int_0^\infty g_1(r^2,\nu)\cdot r^{2m+1}\ dr}{\int_0^\infty g(r^2,\nu)\cdot r^{2m-1}\ dr} \\
\alpha_3 &= \mathrm{E}\Big\{\Big(\frac{g_1(\|\boldsymbol{z}(t)\|^2,\nu)}{g(\|\boldsymbol{z}(t)\|^2,\nu)}\Big)^2\|\boldsymbol{z}(t)\|^4\Big\} \\
&= \int_0^\infty \Big(\frac{g_1(r^2,\nu)}{g(r^2,\nu)}\Big)^2 r^4 g(r^2,\nu)\cdot r^{2m-1}c_{2m}\ dr \\
&= \frac{\int_0^\infty \frac{g_1^2(r^2,\nu)}{g(r^2,\nu)}\cdot r^{2m+3}\ dr}{\int_0^\infty g(r^2,\nu)\cdot r^{2m-1}\ dr} \\
\beta_1 &= \mathrm{E}\Big\{\frac{\frac{\partial g_2(\|\boldsymbol{z}(t)\|^2,\nu)}{\partial\nu}}{g(\|\boldsymbol{z}(t)\|^2,\nu)} - \Big(\frac{g_2(\|\boldsymbol{z}(t)\|^2,\nu)}{g(\|\boldsymbol{z}(t)\|^2,\nu)}\Big)^2\Big\} \\
&= \int_0^\infty \Big\{\frac{\frac{\partial g_2(r^2,\nu)}{\partial\nu}}{g(r^2,\nu)} - \Big(\frac{g_2(r^2,\nu)}{g(r^2,\nu)}\Big)^2\Big\} g(r^2,\nu)\cdot r^{2m-1}c_{2m}\ dr \\
&= \frac{\int_0^\infty \Big\{\frac{\partial g_2(r^2,\nu)}{\partial\nu} - \frac{g_2^2(r^2,\nu)}{g(r^2,\nu)}\Big\}\cdot r^{2m-1}\ dr}{\int_0^\infty g(r^2,\nu)\cdot r^{2m-1}\ dr} \\
\beta_2 &= \mathrm{E}\Big\{\frac{\frac{\partial g_1(\|\boldsymbol{z}(t)\|^2,\nu)}{\partial\nu} g(\|\boldsymbol{z}(t)\|^2,\nu) - g_1(\|\boldsymbol{z}(t)\|^2,\nu) g_2(\|\boldsymbol{z}(t)\|^2,\nu)}{g^2(\|\boldsymbol{z}(t)\|^2,\nu)}\|\boldsymbol{z}(t)\|^2\Big\} \\
&= \int_0^\infty \Big\{\frac{\frac{\partial g_1(r^2,\nu)}{\partial\nu}}{g(r^2,\nu)} - \frac{g_1(r^2,\nu)g_2(r^2,\nu)}{g^2(r^2,\nu)}\Big\} r^2\cdot g(r^2,\nu) r^{2m-1}c_{2m}\ dr \\
&= \frac{\int_0^\infty \Big\{\frac{\partial g_1(r^2,\nu)}{\partial\nu} - \frac{g_1(r^2,\nu)g_2(r^2,\nu)}{g(r^2,\nu)}\Big\}\cdot r^{2m+1}\ dr}{\int_0^\infty g(r^2,\nu)\cdot r^{2m-1}\ dr}
\end{aligned}$$

Gamma Distribution

From the pdf of the gamma distribution (4), we can get the following results easily:

$$\frac{\partial p_u(u;\nu)}{\partial\nu} = \Big(-\mathrm{DG}(\nu) + \ln\nu + 1 + \ln u - u\Big)\cdot p_u(u;\nu), \tag{C.51a}$$

$$\frac{\partial^2 p_u(u;\nu)}{\partial\nu^2} = \Big(-\mathrm{TG}(\nu) + \frac{1}{\nu} + \big(-\mathrm{DG}(\nu) + \ln\nu + 1 + \ln u - u\big)^2\Big)\cdot p_u(u;\nu), \tag{C.52a}$$

where $\mathrm{DG}(x) = \frac{d}{dx}\ln\Gamma(x)$ is the digamma function. For notation simplification, we define $f(u;\nu) = -\mathrm{DG}(\nu) + \ln\nu + 1 + \ln u - u$. In the calculations, we change variables with $x = \nu u$ and use the general Gauss-Leguerre quadrature for both inner and outer integration. The results are

$$\begin{aligned}
\alpha_1 &= \frac{\int_0^\infty \frac{[-\int_0^\infty \exp(-\frac{r^2}{u})u^{-m-1}\cdot\frac{1}{\Gamma(\nu)}\nu^\nu u^{\nu-1}e^{-\nu u}\,du]^2}{\int_0^\infty \exp(-\frac{r^2}{u})u^{-m}\cdot\frac{1}{\Gamma(\nu)}\nu^\nu u^{\nu-1}e^{-\nu u}\,du}\cdot r^{2m+1}\,dr}{\int_0^\infty(\int_0^\infty \exp(-\frac{r^2}{u})u^{-m}\cdot\frac{1}{\Gamma(\nu)}\nu^\nu u^{\nu-1}e^{-\nu u}\,du)\cdot r^{2m-1}\,dr} \\
&= \frac{\int_0^\infty \frac{[-\int_0^\infty \exp(-\frac{r^2\nu}{x})\nu x^{-m-1}\cdot x^{\nu-1}e^{-x}\,dx]^2}{\int_0^\infty \exp(-\frac{r^2\nu}{x})x^{-m}\cdot x^{\nu-1}e^{-x}\,dx}\cdot r^{2m+1}\,dr}{\int_0^\infty(\int_0^\infty \exp(-\frac{r^2\nu}{x})x^{-m}\cdot x^{\nu-1}e^{-x}\,dx)\cdot r^{2m-1}\,dr} \\
&= \frac{\sum_{l_l=1}^{L_{\mathrm{GL}}^{(2m+1)}}\frac{\left(\sum_{l_2=1}^{L_{\mathrm{GL}}^{(\nu-1)}}\exp(-\frac{\nu r_{l_1}^2}{x_{l_2}})\nu x_{l_2}^{-(m+1)}\cdot h_{l_2}\right)^2}{\sum_{l_3=1}^{L_{\mathrm{GL}}^{(\nu-1)}}\exp(-\frac{\nu r_{l_1}^2}{x_{l_3}})x_{l_3}^{-m}\cdot h_{l_3}}\exp(r_{l_1})\cdot h_{l_1}}{\sum_{l_4=1}^{L_{\mathrm{GL}}^{(2m-1)}}\left(\sum_{l_5=1}^{L_{\mathrm{GL}}^{(\nu-1)}}\exp(-\frac{\nu r_{l_4}^2}{x_{l_5}})x_{l_5}^{-m}\cdot h_{l_5}\right)\exp(r_{l_4})\cdot h_{l_4}}.
\end{aligned}$$

Similarly,

$$\begin{aligned}
\alpha_2 &= -\frac{\sum_{l_l=1}^{L_{\mathrm{GL}}^{(2m+1)}}\left(\sum_{l_2=1}^{L_{\mathrm{GL}}^{(\nu-1)}}\exp(-\frac{\nu r_{l_1}^2}{x_{l_2}})\nu x_{l_2}^{-(m+1)}\cdot h_{l_2}\right)\exp(r_{l_1})\cdot h_{l_1}}{\sum_{l_4=1}^{L_{\mathrm{GL}}^{(2m-1)}}\left(\sum_{l_5=1}^{L_{\mathrm{GL}}^{(\nu-1)}}\exp(-\frac{\nu r_{l_4}^2}{x_{l_5}})x_{l_5}^{-m}\cdot h_{l_5}\right)\exp(r_{l_4})\cdot h_{l_4}}, \\
\alpha_3 &= \frac{\sum_{l_l=1}^{L_{\mathrm{GL}}^{(2m+3)}}\frac{\left(\sum_{l_2=1}^{L_{\mathrm{GL}}^{(\nu-1)}}\exp(-\frac{\nu r_{l_1}^2}{x_{l_2}})\nu x_{l_2}^{-(m+1)}\cdot h_{l_2}\right)^2}{\sum_{l_3=1}^{L_{\mathrm{GL}}^{(\nu-1)}}\exp(-\frac{\nu r_{l_1}^2}{x_{l_3}})x_{l_3}^{-m}\cdot h_{l_3}}\exp(r_{l_1})\cdot h_{l_1}}{\sum_{l_4=1}^{L_{\mathrm{GL}}^{(2m-1)}}\left(\sum_{l_5=1}^{L_{\mathrm{GL}}^{(\nu-1)}}\exp(-\frac{\nu r_{l_4}^2}{x_{l_5}})x_{l_5}^{-m}\cdot h_{l_5}\right)\exp(r_{l_4})\cdot h_{l_4}}, \\
\beta_1 &= \frac{\sum_{l_1=1}^{L_{\mathrm{GL}}^{(2m-1)}}\left\{\sum_{l_2=1}^{L_{\mathrm{GL}}^{(\nu-1)}}\exp(-\frac{\nu r_{l_1}^2}{x_{l_2}})x_{l_2}^{-m}\Big(-\mathrm{TG}(\nu)+\frac{1}{\nu}+f^2(\frac{x_{l_2}}{\nu};\nu)\Big)\cdot h_{l_2}\right\}\exp(r_{l_1})\cdot h_{l_1}}{\sum_{l_3=1}^{L_{\mathrm{GL}}^{(2m-1)}}(\sum_{l_4=1}^{L_{\mathrm{GL}}^{(\nu-1)}}\exp(-\frac{\nu r_{l_3}^2}{x_{l_4}})x_{l_4}^{-m}\cdot h_{l_4})\exp(r_{l_3})\cdot h_{l_3}} \\
&\quad -\frac{\sum_{l_5=1}^{L_{\mathrm{GL}}^{(2m-1)}}\frac{[\sum_{l_6=1}^{L_{\mathrm{GL}}^{(\nu-1)}}\exp(-\frac{\nu r_{l_5}^2}{x_{l_6}})x_{l_6}^{-m}\cdot f(\frac{x_{l_6}}{\nu};\nu)\cdot h_{l_6}]^2}{\sum_{l_7=1}^{L_{\mathrm{GL}}^{(\nu-1)}}\exp(-\frac{\nu r_{l_5}^2}{x_{l_7}})x_{l_7}^{-m}\cdot h_{l_7}}\exp(r_{l_5})\cdot h_{l_5}}{\sum_{l_3=1}^{L_{\mathrm{GL}}^{(2m-1)}}(\sum_{l_4=1}^{L_{\mathrm{GL}}^{(\nu-1)}}\exp(-\frac{\nu r_{l_3}^2}{x_{l_4}})x_{l_4}^{-m}\cdot h_{l_4})\exp(r_{l_3})\cdot h_{l_3}}
\end{aligned}$$

and

$$\begin{aligned}
\beta_2 &= -\frac{\sum_{l_1=1}^{L_{\mathrm{GL}}^{(2m+1)}}\left\{\sum_{l_2=1}^{L_{\mathrm{GL}}^{(\nu-1)}}\exp(-\frac{\nu r_{l_1}^2}{x_{l_2}})\nu x_{l_2}^{-m-1}f(\frac{x_{l_2}}{\nu};\nu)\cdot h_{l_2}\right\}\exp(r_{l_1})\cdot h_{l_1}}{\sum_{l_3=1}^{L_{\mathrm{GL}}^{(2m-1)}}(\sum_{l_4=1}^{L_{\mathrm{GL}}^{(\nu-1)}}\exp(-\frac{nur_{l_3}^2}{x_{l_4}})x_{l_4}^{-m}\cdot h_{l_4})e^{r_{l_3}}\cdot h_{l_3}} \\
&\quad +\frac{\sum_{l_5=1}^{L_{\mathrm{GL}}^{(2m+1)}}\frac{\sum_{l_6=1}^{L_{\mathrm{GL}}^{(\nu-1)}}e^{-\frac{\nu r_{l_5}^2}{x_{l_6}}}\nu x_{l_6}^{-(m+1)}h_{l_6}\cdot\sum_{l_7=1}^{L_{\mathrm{GL}}^{(\nu-1)}}e^{-\frac{\nu r_{l_5}^2}{x_{l_7}}}x_{l_7}^{-m}f(\frac{x_{l_7}}{\nu};\nu)h_{l_7}}{\sum_{l_8=1}^{L_{\mathrm{GL}}^{(\nu-1)}}\exp(-\frac{\nu r_{l_5}^2}{x_{l_8}})x_{l_8}^{-m}\cdot h_{l_8}}e^{r_{l_5}}\cdot h_{l_5}}{\sum_{l_3=1}^{L_{\mathrm{GL}}^{(2m-1)}}(\sum_{l_4=1}^{L_{\mathrm{GL}}^{(\nu-1)}}\exp(-\frac{\nu r_{l_3}^2}{x_{l_4}})x_{l_4}^{-m}\cdot h_{l_4})e^{r_{l_3}}\cdot h_{l_3}}.
\end{aligned}$$

Inverse-Gamma Distribution

Fortunately, we have a closed form for the functions of g, g_1, and g_2 in the inverse-gamma distribution with pdf:

$$p_u(u;\nu) = \frac{1}{\Gamma(\nu)}\nu^\nu u^{-\nu-1}e^{-\nu/u} \sim \text{iGamma}(\nu, 1/\nu). \tag{C.53}$$

$$
\begin{aligned}
g(s,\nu) &= \int_0^\infty \exp\Big(-\frac{s}{u}\Big)\cdot u^{-m}\cdot p_u(u;\nu)\ du \\
&= \frac{\Gamma(\nu+m)}{\Gamma(\nu)\nu^m}(1+\frac{s}{\nu})^{-m-\nu}, \qquad \text{(C.54a)} \\
g_1(s,\nu) &= -\int_0^\infty \exp\Big(-\frac{s}{u}\Big)\cdot u^{-m-1}\cdot p_u(u;\nu)\ du, \\
&= -\frac{\Gamma(\nu+m+1)}{\Gamma(\nu)\nu^{m+1}}(1+\frac{s}{\nu})^{-m-\nu-1} \qquad \text{(C.54b)}
\end{aligned}
$$

and

$$
\begin{aligned}
g_2(s,\nu) &= \frac{\partial g(s,\nu)}{\partial \nu} \\
&= \Big(\mathrm{DG}(\nu+m)-\mathrm{DG}(\nu)-\frac{m}{\nu}-\ln(1+\frac{s}{\nu})+\frac{(m+\nu)s}{\nu^2(1+\frac{s}{\nu})}\Big)\cdot g(s,\nu). \qquad \text{(C.54c)}
\end{aligned}
$$

The calculations yield

$$
\begin{aligned}
\alpha_1 &= \frac{m(\nu+m)}{\nu+m+1}; \qquad \text{(C.55a)} \\
\alpha_2 &= -m; \qquad \text{(C.55b)} \\
\alpha_3 &= \frac{m(m+1)(\nu+m)}{\nu+m+1}; \qquad \text{(C.55c)} \\
\beta_1 &= \mathrm{TG}(\nu+m)-\mathrm{TG}(\nu)+\frac{m(\nu+m+2)}{\nu(\nu+m)(\nu+m+1)}; \qquad \text{(C.55d)} \\
\beta_2 &= -\frac{m}{(\nu+m)(\nu+m+1)}, \qquad \text{(C.55e)}
\end{aligned}
$$

APPENDIX D
HYBRID-CRB (HCRB)

A. General Results

In the compound-Gaussian model,

$$
\begin{aligned}
\boldsymbol{y}(t)|u(t) &\sim p_{\boldsymbol{y}|u}(\boldsymbol{y}(t)|u(t);X,\Sigma) \\
&= \frac{1}{|\pi u(t)\Sigma|}\exp\{-[\boldsymbol{y}(t)-AX\boldsymbol{\phi}(t)]^H\cdot[u(t)\Sigma]^{-1}\cdot[\boldsymbol{y}(t)-AX\boldsymbol{\phi}(t)]\}, \qquad \text{(D.56a)} \\
u(t) &\sim p_u(u(t);\nu). \qquad \text{(D.56b)}
\end{aligned}
$$

The complete data log-likelihood function is

$$
\mathcal{L}=\sum_{t=1}^{N}\Big\{-\ln|\Sigma|-[\boldsymbol{y}(t)-AX\phi(t)]^H\cdot\frac{\Sigma^{-1}}{u(t)}\cdot[\boldsymbol{y}(t)-AX\phi(t)]+\ln p_u(u(t);\nu)\Big\}. \qquad \text{(D.57)}
$$

Let $\boldsymbol{z}(t)=\Sigma^{-\frac{1}{2}}\cdot\frac{\boldsymbol{y}(t)-AX\phi(t)}{\sqrt{u(t)}}, \quad t=1,\ldots,N$. $\boldsymbol{z}$ is SIRV.

1) Expectations: Since,

$$p_{z|u}(\boldsymbol{z}(t)|u(t);X,\Sigma)=\frac{1}{\pi^m}\exp\{-\|\boldsymbol{z}(t)\|^2\} \tag{D.58}$$

Similarly to Appendix C, we build a map $\mathbb{C}^m:\boldsymbol{z}\rightarrow\mathbb{R}^{2m}:\boldsymbol{w}$. Then

$$\begin{aligned}\|\boldsymbol{z}\| &= \|\boldsymbol{w}\|, &\text{(D.59a)}\\ p_w(\boldsymbol{w};\nu) &= \frac{1}{\pi^m}\exp(-\|\boldsymbol{w}\|^2). &\text{(D.59b)}\end{aligned}$$

$$\mathrm{E}_{\boldsymbol{y}|u}(1)=1\Longrightarrow\int_0^\infty\exp(-r^2)\cdot r^{2m-1}\,dr=\frac{\pi^m}{c_{2m}}. \tag{D.60}$$

It is not hard to get

$$\begin{aligned}\mathrm{E}_{\boldsymbol{y}|u}(\|\boldsymbol{z}\|^2) &= m, &\text{(D.61a)}\\ \mathrm{E}_{\boldsymbol{y}|u}(\|\boldsymbol{z}\|^4) &= m(m+2), &\text{(D.61b)}\end{aligned}$$

where the recurrence relation $c_{k+2}=\frac{2\pi c_k}{k}$ is used. Here c_k is the surface area of a unit ball in $\mathbb{R}^k$.

Before deriving the entries of the FIM, we note that the first order partial derivatives are

$$\begin{aligned}\frac{\partial\mathcal{L}}{\partial\xi_i} &= \sum_{t=1}^N\frac{\partial l(t)}{\partial\xi_i}\\ &= \sum_{t=1}^N\Big\{\boldsymbol{z}^H(t)\cdot\frac{\Sigma^{-\frac{1}{2}}}{\sqrt{u(t)}}\cdot A\frac{\partial X}{\partial\xi_i}\phi(t)+\phi^H(t)\frac{\partial X^H}{\partial\xi_i}A^H\cdot\frac{\Sigma^{-\frac{1}{2}}}{\sqrt{u(t)}}\cdot\boldsymbol{z}(t)\Big\} &\text{(D.62a)}\\ \frac{\partial\mathcal{L}}{\partial\eta_i} &= \sum_{t=1}^N\frac{\partial l(t)}{\partial\eta_i}\\ &= -N\cdot\mathrm{tr}(\Sigma^{-1}\frac{\partial\Sigma}{\partial\eta_i})+\sum_{t=1}^N\boldsymbol{z}^H(t)\cdot\Sigma^{-\frac{1}{2}}\frac{\partial\Sigma}{\partial\eta_i}\Sigma^{-\frac{1}{2}}\cdot\boldsymbol{z}(t) &\text{(D.62b)}\\ \frac{\partial\mathcal{L}}{\partial\nu} &= \sum_{t=1}^N\frac{\partial l(t)}{\partial\nu}\\ &= \sum_{t=1}^N\frac{1}{p_u(u(t);\nu)}\frac{\partial p_u(u(t);\nu)}{\partial\nu}. &\text{(D.62c)}\end{aligned}$$

We follow the same procedure of Appendix B and get (see [32] for details)

$$
\begin{aligned}
I_{\xi_i\xi_j} &= \mathrm{E}_u\Big\{\mathrm{E}_{\boldsymbol{y}|u}\{\frac{\partial\mathcal{L}}{\partial\xi_i}\frac{\partial\mathcal{L}}{\partial\xi_j}\}\Big\} \\
&= 2\sum_{t=1}^{N}\mathrm{Re}\Big[\mathrm{tr}(A\frac{\partial X}{\partial\xi_i}\phi(t)\cdot\phi^H(t)\frac{\partial X^H}{\partial\xi_i}A^H\Sigma^{-1})\Big]\cdot\mathrm{E}_u\{u^{-1}(t)\} \qquad \text{(D.63a)} \\
I_{\eta_i\eta_j} &= \mathrm{E}_u\Big\{\mathrm{E}_{\boldsymbol{y}|u}\{\frac{\partial\mathcal{L}}{\partial\eta_i}\frac{\partial\mathcal{L}}{\partial\eta_j}\}\Big\} \\
&= \frac{N(m+2)}{(m+1)}\mathrm{tr}(\Sigma^{-1}\frac{\partial\Sigma}{\partial\eta_i}\Sigma^{-1}\frac{\partial\Sigma}{\partial\eta_j}) \qquad \text{(D.63b)} \\
I_{\nu\nu} &= -\mathrm{E}_u\Big\{\frac{\partial^2\mathcal{L}}{\partial\nu^2}\Big\} \\
&= -\sum_{t=1}^{N}\mathrm{E}_u\Big\{\frac{1}{p_u}\frac{\partial^2 p_u}{\partial\nu^2}-\frac{1}{p_u^2}\Big(\frac{\partial p_u}{\partial\nu}\Big)^2\Big\}, \qquad \text{(D.63c)}
\end{aligned}
$$

where $c_{\eta_i\eta_j}=\mathrm{tr}(\Sigma^{-1}\frac{\partial\Sigma}{\partial\eta_i})\,\mathrm{tr}(\Sigma^{-1}\frac{\partial\Sigma}{\partial\eta_j})$, and

$$
I_{\eta_i\nu} = I_{\xi_i\nu} = 0. \qquad \text{(D.63d)}
$$

B. Application to Specific Texture Distributions

1) Gamma Distribution: From gamma pdf

$$
p_u(u(t);\nu)=\frac{1}{\Gamma(\nu)}\nu^\nu u(t)^{\nu-1}e^{-\nu u(t)}\sim\text{Gamma}(\nu,1/\nu). \qquad \text{(D.64)}
$$

We can derive $\mathrm{E}_u(u^{-1}(t))=\frac{1}{\theta(\alpha-1)}=\frac{\nu}{\nu-1}$. Also,

$$
\begin{aligned}
\frac{\partial p_u}{\partial\nu} &= \Big(-\mathrm{DG}(\nu)+\ln\nu+1+\ln u(t)-u(t)\Big)\cdot p_u, \qquad \text{(D.65a)} \\
\frac{\partial^2 p_u}{\partial\nu^2} &= \Big(-\mathrm{TG}(\nu)+\frac{1}{\nu}+\big(-\mathrm{DG}(\nu)+\ln\nu+1+\ln u(t)-u(t)\big)^2\Big)\cdot p_u. \qquad \text{(D.65b)}
\end{aligned}
$$

Substitute the above results into (D.63a) and (D.63c), we get,

$$
\begin{aligned}
I_{\xi_i\xi_j} &= \frac{2\nu}{\nu-1}\cdot\sum_{t=1}^{N}\mathrm{Re}\Big[\mathrm{tr}(A\frac{\partial X}{\partial\xi_i}\phi(t)\cdot\phi^H(t)\frac{\partial X^H}{\partial\xi_i}A^H\Sigma^{-1})\Big], \qquad \text{(D.66a)} \\
I_{\eta_i\eta_j} &= \frac{N(m+2)}{(m+1)}\cdot\mathrm{tr}(\Sigma^{-1}\frac{\partial\Sigma}{\partial\eta_i}\Sigma^{-1}\frac{\partial\Sigma}{\partial\eta_j}), \qquad \text{(D.66b)} \\
I_{\nu\nu} &= N\cdot\mathrm{TG}(\nu)-\frac{N}{\nu}. \qquad \text{(D.66c)}
\end{aligned}
$$

2) Inverse Gamma Distribution (t-Distributed Clutter):

$$
p_u(u(t);\nu)=\frac{1}{\Gamma(\nu)}\nu^\nu u(t)^{-\nu-1}e^{-\nu/u(t)}\sim\text{iGamma}(\nu,1/\nu). \qquad \text{(D.67)}
$$

$$
\mathrm{E}_u\{u^{-1}(t)\}=\alpha\theta=1. \qquad \text{(D.68)}
$$

and

$$\frac{\partial p_u}{\partial \nu} = \Big(- \mathrm{DG}(\nu) + \ln \nu + 1 - \ln u(t) - \frac{1}{u(t)} \Big) \cdot p_u, \quad \text{(D.69a)}$$

$$\frac{\partial^2 p_u}{\partial \nu^2} = \Big(- \mathrm{TG}(\nu) + \frac{1}{\nu} + \big(- \mathrm{DG}(\nu) + \ln \nu + 1 - \ln u(t) - \frac{1}{u(t)} \big)^2 \Big) \cdot p_u. \quad \text{(D.69b)}$$

Thus,

$$I_{\xi_i \xi_j} = 2 \cdot \sum_{t=1}^{N} \mathrm{Re} \Big[\mathrm{tr}(A \frac{\partial X}{\partial \xi_i} \phi(t) \cdot \phi^H(t) \frac{\partial X^H}{\partial \xi_i} A^H \Sigma^{-1}) \Big], \quad \text{(D.70a)}$$

$$I_{\eta_i \eta_j} = \frac{N(m+2)}{(m+1)} \cdot \mathrm{tr}(\Sigma^{-1} \frac{\partial \Sigma}{\partial \eta_i} \Sigma^{-1} \frac{\partial \Sigma}{\partial \eta_j}), \quad \text{(D.70b)}$$

$$I_{\nu\nu} = N \cdot \mathrm{TG}(\nu) - \frac{N}{\nu}. \quad \text{(D.70c)}$$

Interestingly, the inverse-gamma texture and the gamma texture share the same block in the FIM of $\boldsymbol{\eta}$ and ν.

REFERENCES

[1] H. Goldstein, "Sea echo," in *Propagation of Short Radio Waves*, D. E. Kerr, Ed. New York: McGraw-Hill, pp. 481-527, 1951.

[2] F. Gini, M. V. Greco, M. Diani, and L. Verrazzani, "Performance analysis of two adaptive radar detectors against non-Gaussian real sea clutter data," *IEEE Trans. Aerosp. Electron. Syst.*, vol. 36, pp. 1429-1439, Oct. 2000.

[3] K. J. Sangston and K. R. Gerlach, "Coherent detection of radar targets in a non-Gaussian background," *IEEE Trans, on Aerospace and Electronic Systems*, vol. 30, pp. 330-340, April 1994.

[4] S. Haykin, R. Bakker, and B. W. Currie, "Uncovering nonlinear dynamics – The case study of sea clutter," *Proc. IEEE*, vol. 90, pp. 860-881, May 2002.

[5] G. R. Valenzula, "Theories for the interaction of electromagnetic waves and oceanic waves – A review," *Bound. Layer Meteorol.*, vol. 13, no. 1/4, pp. 61-65, 1978.

[6] M. Greco, F. Bordoni, and F. Gini, "X-band sea-clutter nonstationarity: Influence of long waves," *IEEE Journal of Oceanic Engineering*, vol. 29, No. 2, pp. 269-283, Apr. 2004.

[7] F. G. Bass, I. M. Fuks, A. E. Kalmykov, I. E. Ostrovsky, and A. D. Rosenberg, "Very high frequency radiowave scattering by a disturbed sea surface," *IEEE Trans. Antennas Propagat.*, vol, AP-16, pp. 554-568, 1968.

[8] J. W. Wright, "A new model for sea clutter," *IEEE Trans. Antennas Propagat.*, vol. AP-16, pp. 217-223, 1968.

[9] E. Jakeman and P. N. Pusey, "A model for non-Rayleigh sea echo," *IEEE Trans. Antennas and Propagation*, vol. 24, no. 6, pp. 806-814, Nov. 1976.

[10] K. Yao, "Spherically invariant random processes: Theory and applications," in *Communications, Information and Network Security*, V.K. Bhargava *et al.*, Eds., Dordrecht, the Netherlands: Kluwer Academic Publishers, pp. 315-332, 2002.

[11] E. J. Kelly and K. M. Forsythe, *Adaptive detection and parameter estimation for multidimensional signal models*, Lincoln Laboratory, Tech. Report 848, April 1989.

[12] A. Dogandžić and A. Nehorai, "Generalized multivariate analysis of variance: A unified framework for signal processing in correlated noise," *IEEE Signal Processing Mag.*, vol. 20, pp. 39–54, Sept. 2003.

[13] E. Conte, and A. De Maio, "Distributed target detection in compound-Gaussian noise with Rao and Wald tests," *IEEE Trans. Aerosp. Electron. Syst.*, vol. 39, pp. 568-582, Apr. 2003.

[14] V. Anastassopoulos, G. A. Lampropoulos, A. Drosopoulos, and N. Rey, "High resolution radar clutter statistics," *IEEE Trans. Aerosp. Electron. Syst.*, vol. 35, pp. 43-60, Jan. 1999.

[15] M. Rangaswamy and J. H. Michels, "Adaptive signal processing in non-Gaussian noise backgrounds," in *Proc. 9th IEEE SSAP Workshop,* Portland, OR, Sept. 1998, pp. 53-56.

[16] M. Rangaswamy, J. H. Michels, and B. Himed, "Statistical analysis of the nonhomogeneity detector for non-Gaussian interference backgrounds," *Proc. IEEE Radar Conf.*, Long Beach, CA, Apr. 2002, pp. 304-310.

[17] M. Rangaswamy, D. D. Weiner, and A. Ozturk, "Non-Gaussian random vector identification using spherically invariant random processes," *IEEE Trans. Aerosp. Electron. Syst.*, vol. 29, pp. 111-123, Jan. 1993.

[18] F. Gini, and A. Farina, "Vector subspace detection in compound-Gaussian clutter. Part I: survey and new results," *IEEE Trans. Aerosp. Electron. Syst.*, vol. 38, No. 4, pp. 1295-1311, Oct. 2002.

[19] K. L. Lange, R. J. A. Little, and J. M. G. Taylor, "Robust statistical modeling using the t distribution," *J. Amer. Stat. Assoc.*, vol. 84, pp. 881-896, Dec. 1989.

[20] E. Jay, J.P. Ovarlez, D. Declercq, and P. Duvaut, "Bayesian optimum radar detector in non-Gaussian noise," *IEEE International Conference on Acoustics, Speech, and Signal Processing, 2002. Proceedings. (ICASSP '02).*, 2002, pp. 1289-1292.

[21] E. Jay, J. P. Ovarlez, D. Declercq, and P. Duvaut, "BORD: Bayesian optimum radar detector," *Signal Processing*, vol. 83, no. 6, pp. 1151-1162, 2003.

[22] A. Dogandžić, A. Nehorai, and J. Wang, "Maximum likelihood estimation of compound-Gaussian clutter and target parameters," in *Proc. 12th Ann. Workshop Adaptive Sensor Array Processing (ASAP '04)*, Lincoln Laboratory, Lexington, MA, Mar. 2004.

[23] C. H. Liu, D. B. Rubin, and Y. N. Wu, "Parameter expansion to accelerate EM: The PX-EM algorithm," *Biometrika*, vol. 85, pp. 755-770, Dec. 1998.

[24] M. K. Simon and M.-S. Alouini, *Digital Communication over Fading Channels*, New York: Wiley, 2000.

[25] P.J. Bickel and K.A. Doksum, *Mathematical Statistics: Basic Ideas and Selected Topics*, 2nd ed., Upper Saddle River, NJ:Prentice Hall, 2000.

[26] A. Dogandžić and J. Jin, "Estimating statistical properties of composite gamma-lognormal fading channels," in *Proc. Globecom Conf.*, San Francisco, CA, Dec. 2003, pp. 2406–2410.

[27] R.A. Thisted, *Elements of Statistical Computing: Numerical Computation*, New York: Chapman & Hall, 1988.

[28] J. Wang, A. Dogandžić, and A. Nehorai, "Cramer-Rao bounds for compound-Gaussian clutter and target parameters," *IEEE Int. Conf. Acoust., Speech, Signal Processing*, Philadelphia, PA, Mar. 2005. pp. 1101-1104.

[29] S. M. Kay, *Fundamentals of Statistical Signal Processing: Estimation Theory*, PTR Prentice-Hall, Inc. New Jersey, 1993.

[30] F. Gini, R. Reggiannini, "On the use of Cramér-Rao-like bounds in the presence of random nuisance parameters," *IEEE Trans. Communications*, vol. 48, pp. 2120-2126, Dec. 2000.

[31] J. Ward, *Space-Time Adaptive Processing for Airborne Radar,* Lincoln Lab., Tech. Report 1015, MIT, Dec, 1994.

[32] J. Wang, A. Dogandžić, and A. Nehorai, *Parameter estimation and detection for compound-Gaussian clutter models*, Dept. Elect. and Comput. Eng., Univ. Illinois at Chicago, Rep. UIC-ECE-05-5, Apr. 2005.

[33] M. Viberg, P. Stoica, and B. Ottersten, "Maximum likelihood array processing in spatially correlated noise fields using parameterized signals," *IEEE Trans. Signal Processing,* vol. 45, pp. 996–1004, Apr. 1997.

LIST OF FIGURES

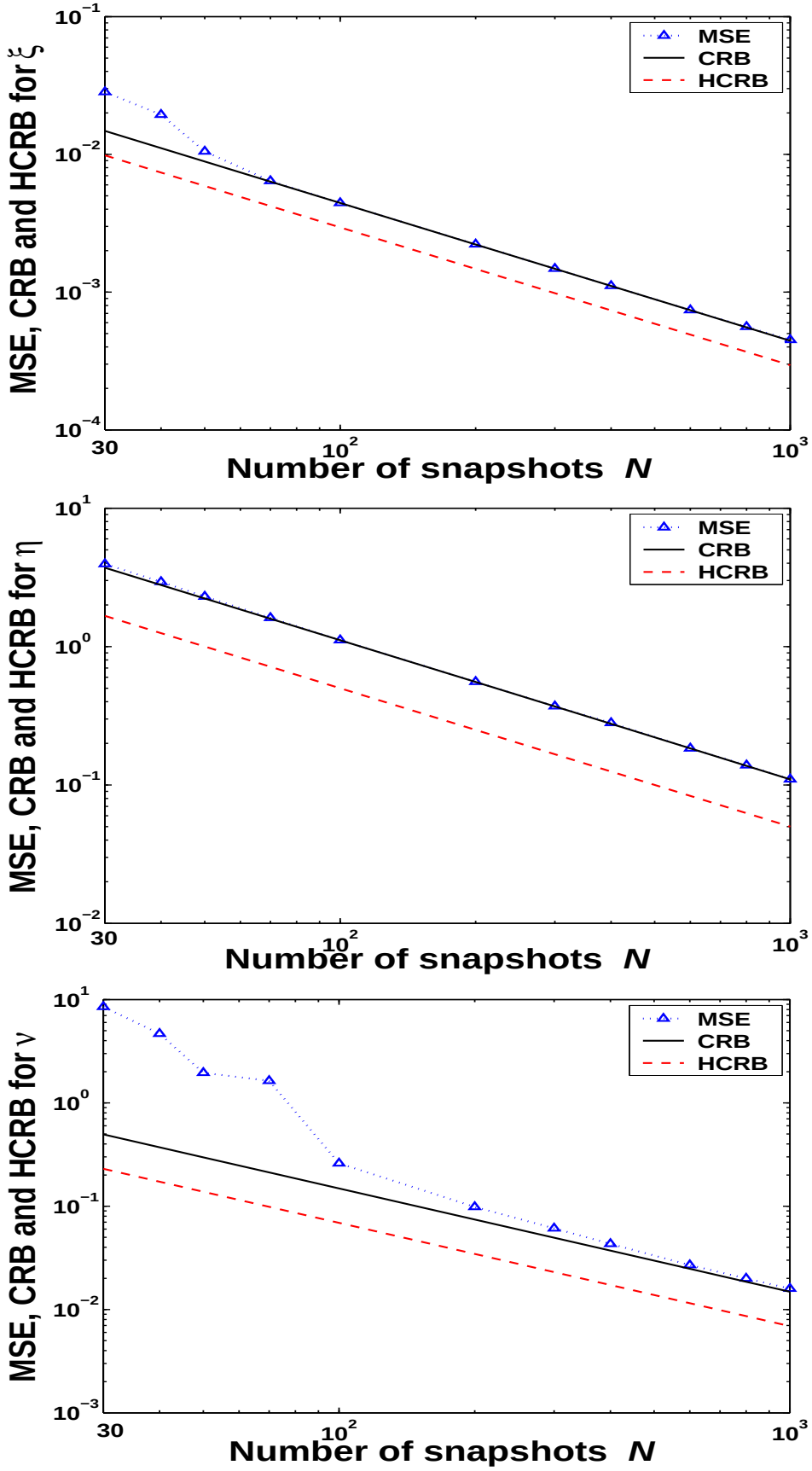

Fig. 1. Average MSEs for the ML estimates of ξ, η, ν and corresponding CRBs and HCRBs under the gamma texture model, as functions of N.

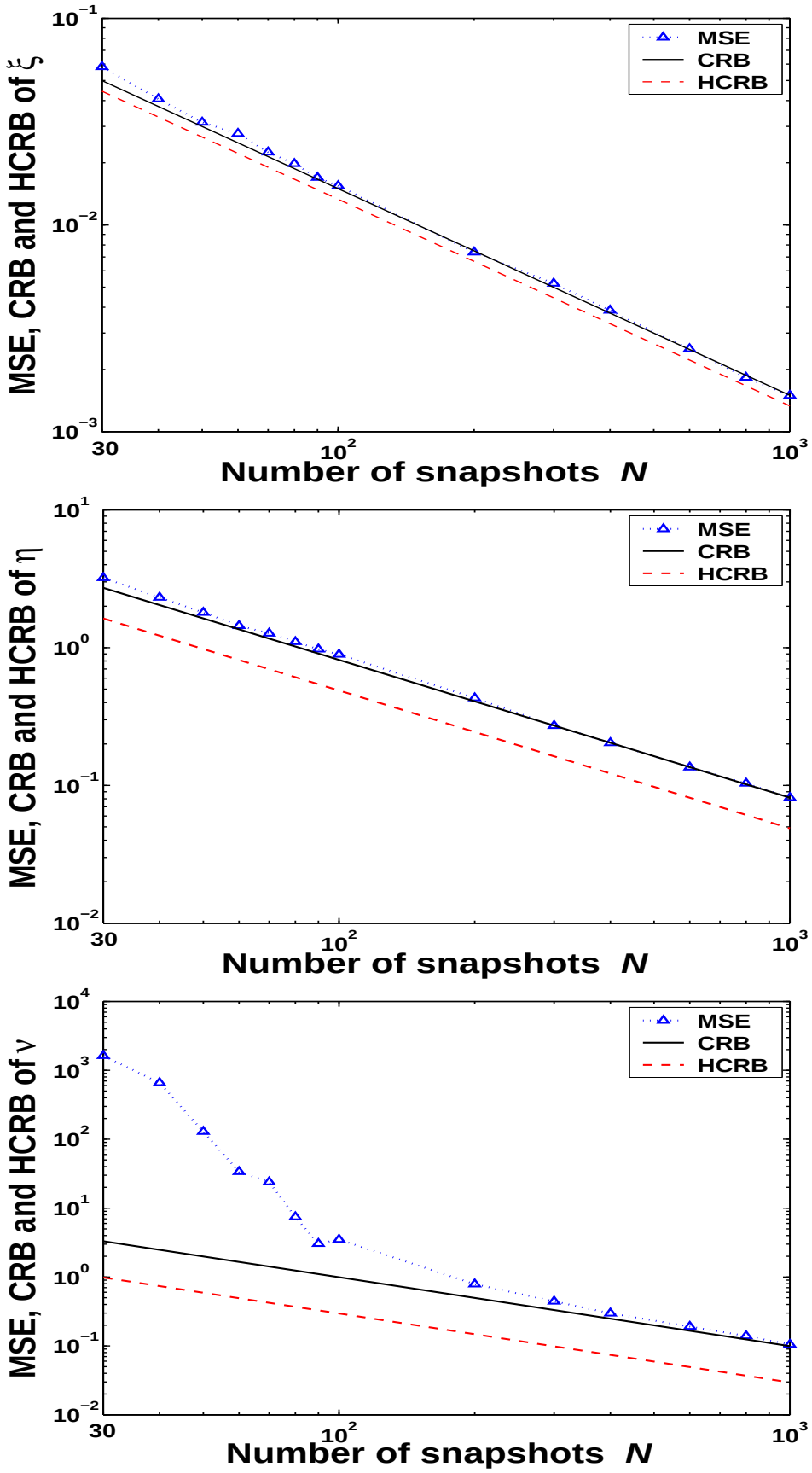

Fig. 2. Average MSEs for the ML estimates of $\boldsymbol{\xi}, \boldsymbol{\eta}, \nu$ and corresponding CRBs and HCRBs under the inverse-gamma texture model, as functions of N.

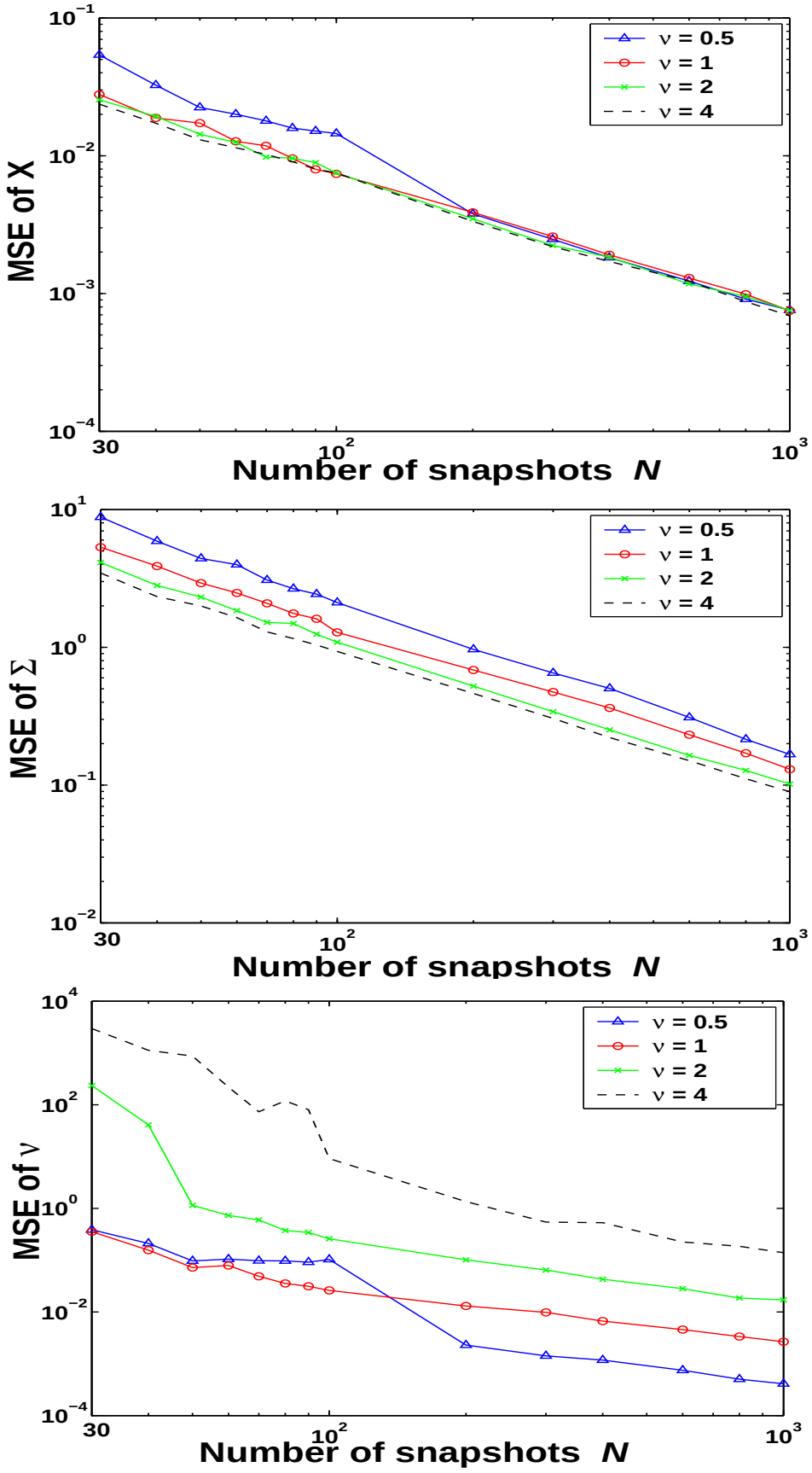

Fig. 3. Average MSEs for the ML estimates of ξ, η, ν under the inverse-gamma texture model as functions of N for different ν values.